A simulation method to infer tree allometry and forest structure from airborne laser scanning and forest inventories

Fabian Jörg Fischer, Fabian Jörg Fischer, Nicolas Labrière, Grégoire Vincent, Bruno Hérault, Alfonso Alonso, Hervé Memiaghe, Pulchérie Bissiengou, David Kenfack, Sassan Saatchi, et al.

A simulation method to infer tree allometry and forest structure from airborne laser scanning and forest inventories

Fabian Jörg Fischer[a,*], Nicolas Labrière[a], Grégoire Vincent[b], Bruno Hérault[c,d], Alfonso Alonso[e], Hervé Memiaghe[f], Pulchérie Bissiengou[g], David Kenfack[h], Sassan Saatchi[i], and Jérôme Chave[a]

[a] Laboratoire Évolution et Diversité Biologique, UMR 5174 (CNRS/IRD/UPS), 118 Route de Narbonne, 31062 Toulouse Cedex 9, France

[b] AMAP, Univ Montpellier, IRD, CIRAD, CNRS, INRAE, Montpellier, France

[c] Cirad, Univ Montpellier, UR Forests & Societies, F-34000 Montpellier, France.

[d] INPHB, Institut National Polytechnique Félix Houphouët-Boigny, Yamoussoukro, Ivory Coast

[e] Center for Conservation and Sustainability, Smithsonian Conservation Biology Institute, 1100 Jefferson Drive SW, Suite 3123, Washington DC 20560-0705, USA

[f] Institut de Recherche en Écologie Tropicale (IRET), Centre National de la Recherche Scientifique et Technologique (CENAREST), B.P. 13354, Libreville, Gabon

[g] Institut de Pharmacopée et de Médecine Traditionnelles (IPHAMETRA)/Herbier National du Gabon, Centre National de la Recherche Scientifique et Technologique (CENAREST), B.P. 1165, Libreville, Gabon

[h] Center for Tropical Forest Science -Forest Global Earth Observatory, Smithsonian Tropical Research Institute, West Loading Dock, 10th and Constitution Ave NW, Washington DC 20560, USA

[i] Jet Propulsion Laboratory, California Institute of Technology, 4800 Oak Grove Drive, Pasadena, CA 91109, USA

* Correspondence: fabian.j.d.fischer@gmx.de

Keywords: vegetation structure; tropical forest; individual-based modeling; airborne lidar; approximate bayesian computation; allometry; biomass; canopy space filling

Abstract

Tropical forests are characterized by large carbon stocks and high biodiversity, but they are increasingly threatened by human activities. Since structure strongly influences the functioning and resilience of forest communities and ecosystems, it is important to quantify it at fine spatial scales.

Here, we propose a new simulation-based approach, the "Canopy Constructor", with which we quantified forest structure and biomass at two tropical forest sites, one in French Guiana, the other in Gabon. In a first step, the Canopy Constructor combines field inventories and airborne lidar scans to create virtual 3D representations of forest canopies that best fit the data. From those, it infers the forests' structure, including crown packing densities and allometric scaling relationships between tree dimensions. In a second step, the results of the first step are extrapolated to create virtual tree inventories over the whole lidar-scanned area.

Across the French Guiana and Gabon plots, we reconstructed empirical canopies with a mean absolute error of 3.98m [95% credibility interval: 3.02, 4.98], or 14.4%, and a small upwards bias of 0.66m [-0.41, 1.8], or 2.7%. Height-stem diameter allometries were inferred with more precision than crown-stem diameter allometries, with generally larger heights at the Amazonian than the African site, but similar crown-stem diameter allometries. Plot-based aboveground biomass was inferred to be larger in French Guiana with 400.8 t ha^{-1} [366.2 – 437.9], compared to 302.2 t ha^{-1} in Gabon [267.8 – 336.8] and decreased to 299.8 t ha^{-1} [275.9 – 333.9] and 251.8 t ha^{-1} [206.7 – 291.7] at the landscape scale, respectively. Predictive accuracy of the extrapolation procedure had an RMSE of 53.7 t ha^{-1} (14.9%) at the 1 ha scale and 87.6 t ha^{-1} (24.2%) at

54 the 0.25 ha scale, with a bias of -17.1 t ha^{-1} (-4.7%). This accuracy was similar to
55 regression-based approaches, but the Canopy Constructor improved the representation
56 of natural heterogeneity considerably, with its range of biomass estimates larger by
57 54% than regression-based estimates.
58
59 The Canopy Constructor is a comprehensive inference procedure that provides fine-
60 scale and individual-based reconstructions even in dense tropical forests. It may thus
61 prove vital in the assessment and monitoring of those forests, and has the potential for a
62 wider applicability, for example in the exploration of ecological and physiological
63 relationships in space or the initialisation and calibration of forest growth models.

1. Introduction

Tropical forests store more than half of terrestrial living biomass (Pan et al., 2011) and shelter a disproportionate share of terrestrial biodiversity. Yet they are increasingly threatened by human activities, from agricultural encroachment and fragmentation to global climate change (Lewis et al., 2015). Tropical forests thus play a pivotal role in carbon mitigation and conservation strategies such as natural regeneration and the avoidance of deforestation (Chazdon et al., 2016; Grassi et al., 2017). To prioritize such strategies and assess their efficacy, methods are needed that accurately quantify forest structure, i.e. the vertical and horizontal arrangement of tree stems and crowns.

Forest structure shapes ecosystem functioning (Shugart et al., 2010), wood quality (Van Leeuwen et al., 2011), microclimates and habitats (Davis et al., 2019), and the resilience and resistance of ecosystems to disturbances (DeRose and Long, 2014; Seidl et al., 2014; Tanskanen et al., 2005). Forest structure also varies across climates (Pan et al., 2013) and across successional states and environmental conditions (Lutz et al., 2013). Approaches to quantify forest structure should therefore be able to account for local heterogeneities and be applicable over large areas (R. Fischer et al., 2019).

Field-based inventories provide detailed descriptions of diameter distributions across time and space and form the bedrock of research in forest ecology. However, the mapping, measuring and identification of trees is typically limited to a few hectares. Furthermore, it is usually difficult to obtain reliable measurements of tree height and other crown dimensions from the ground (Sullivan et al., 2018). As a result, it has long been a challenge to correctly describe the three-dimensional stratification of forests (Oldeman, 1974).

Much has changed, however, with the advent of laser scanning and its ability to obtain data in three dimensions (Atkins et al., 2018; Disney, 2019). At regional scales, airborne laser scanning (ALS), i.e. aircraft-mounted laser scanning devices, are now commonly used to survey forest stratification over thousands of hectares. The data can be used to infer canopy height and leaf density at sub-meter resolution (Riaño et al., 2004; Rosette et al., 2008; Vincent et al., 2017), with diverse purposes, from estimating carbon stocks (Asner and Mascaro, 2014) to mapping animal habitats (Goetz et al., 2010). In some situations, even individual tree dimensions – especially tree height, crown area and depth – can be deduced by segmenting dense ALS point clouds into individual plants and their components (Aubry-Kientz et al., 2019; Ferraz et al., 2016; Hyyppä and Inkinen, 1999; Morsdorf et al., 2004). In particular for emergent and more loosely spaced trees, full crowns are often visible in ALS datasets and can be monitored from above (Levick and Asner, 2013; Meyer et al., 2018; Stovall et al., 2019). While this technique has been well-researched in temperate and boreal forests, its implementation is more difficult in the multistoried forests typically found in the tropics. In the latter case, many trees are overtopped and difficult to delineate, so a large part of the information on individual tree size is inaccessible. Furthermore, even when tree crowns have been isolated, the matching of crowns to ground-measured diameters is made difficult by asymmetries in tree growth and uncertainties in geo-positioning.

Here we propose an alternative, simulation-based strategy to infer forest structure. It relies on a combination of ALS data and field inventories to first reconstruct forests in 3D on local field plots, and then uses local summary statistics to create virtual tree inventories over the whole ALS-extent. We call our method the "Canopy Constructor". It is inspired by the fusion of forest simulators with lidar data (Fassnacht et al., 2018; F. J. Fischer et al., 2019; Hurtt et al., 2004; Knapp et al., 2018; Shugart et al.,

112 2015), space-filling algorithms (Bohn and Huth, 2017; Farrior et al., 2016; Taubert et al.,
113 2015) and the use of synthetic forests to link lidar and ground inventories (Palace et al.,
114 2015; Spriggs et al., 2015). The Canopy Constructor brings these approaches together to
115 provide a comprehensive picture of forest canopies in space, with applications in
116 biomass mapping, the study of remote sensing techniques and the initialization or
117 calibration of forest growth models (F. J. Fischer et al., 2019).
118 To implement it, we used the assumptions of the spatially explicit and individual-
119 based forest growth model TROLL (Maréchaux and Chave 2017) and notions from
120 allometric scaling theories, i.e. that tree dimensions can be predicted through allometric
121 relationships (Niklas 2007) and that space-filling concepts translate between the
122 properties of individual trees and those of the whole stand (Niklas et al., 2003; West et
123 al., 2009). Unlike general theories of allometric scaling, however, the Canopy
124 Constructor seeks to infer realized scaling relationships from local plot data, and then
125 uses these to predict tree positions and dimensions in space.
126 Here, we describe the Canopy Constructor algorithm, and apply it at two tropical
127 rain forest sites, one in French Guiana (Chave et al., 2008a), one in Gabon (Memiaghe et
128 al., 2016), to infer the allometric relationships between trunk diameter and crown
129 dimensions, and to create virtual tree inventories across several thousands of hectares,
130 from which fine-scale above-ground biomass maps can be deduced. Specifically, we
131 asked the following questions: (i) How well can we reproduce 3D scenes of tropical
132 forests from relatively simple principles, (ii) Are tree inventories and ALS data sufficient
133 to infer allometric scaling relationships between tree dimensions, and how do these
134 relationships differ between sites? (iii) What is the biomass density at both sites and
135 how is it distributed across the landscape? (iv) How accurate is the Canopy Constructor
136 approach in extrapolation and does it have an advantage over conventional biomass

mapping methods? We evaluated the Canopy Constructor's predictions through independent data and cross-validation, compared the accuracy against regression-based approaches, and, for practical purposes, provide an assessment of its accuracy with a reduced set of simulations.

2. Materials and Methods

2.1 Study sites

To answer our research questions, we selected two tropical sites, one in French Guiana, and one in Gabon. The two sites were chosen based on their location in the Earth's two largest tropical forest biomes, with high biomass and biodiversity, which makes it a challenge to correctly estimate their structure. Furthermore, their biomass has been recently quantified, so we had empirical data sets and estimates at hand to compare our approach with (Labriere et al., 2018). Throughout, we refer to them as study sites, while tree inventories are referred to as plots.

The French Guiana site is the Nouragues Ecological Research Station (4.06°N, 52.68°W). The site is characterised by a lowland tropical rainforest (except for a granitic outcrop at 430m asl), ca. 2900 mm yr^{-1} rainfall, a 3-month dry season in September-November, and a shorter one in March. Its forest forms part of the Guiana Shield, at the northeastern tip of Amazonia, a region with high tree wood densities and biomass, and a large fraction of legume species (ter Steege et al., 2006). Tree inventories have been carried out since 1992, including a 10-ha plot called "Grand Plateau" and a 12-ha plot called "Petit Plateau" (Chave et al., 2008b). Trees with diameters ≥ 10 cm at 1.30m above the ground (diameter at breast height, dbh) or above deformities and buttresses are mapped, tagged and identified at species level when possible. The two plots differ in their disturbance regime and canopy structure (cf. Figure S1 for their canopy height models), but a typical hectare includes between 500 and 600 trees ≥ 10cm dbh and ≥ 150 tree species. Dominant species are *Eschweilera coriacea*, *Quararibea duckei*, *Lecythis persistens*, *Vouacapoua americana*, *Eperua falcata* and the palm *Astrocaryum sciophilum* (Poncy et al., 2001). Several ALS surveys have been conducted since 2008 (Réjou-Méchain et al., 2015), with a Riegl lidar (LMS-Q560) mounted on a fixed-wing aircraft.

We here used the 2012 tree inventory and ALS dataset which covers 2,400 ha at a pulse density of ~12 per m^2 (based on density of last returns) and an overall point density of ~18 per m^2 (all returns; Réjou-Méchain *et al.*, 2015).

The second site, Rabi, is located in southwestern Gabon's Gamba Complex, (1.92°S, 9.88°E). The site is characterized by annual rainfall of ca. 1970 mm yr^{-1} (Anderson-Teixeira et al., 2015a), and is covered with a lowland old-growth tropical rain forest, with local human disturbances by oil operations and selective logging. A 25 ha plot has been censused twice, including all trees ≥ 1 cm dbh, in 2010-2012 and 2016-2017 (Memiaghe et al., 2016), following the ForestGEO protocol (Condit, 1998). The plot has an estimated 84 species ha^{-1} and 447 trees ≥ 10 cm dbh ha^{-1} (Memiaghe et al., 2016). The legume family contributes a large fraction of species, trees and biomass, with four species, *Tetraberlinia moreliana*, *Tetraberlinia bifoliolata*, *Gilbertiodendron ogoouense*, and *Amanoa strobilaceae*, accounting for ca. 45% of canopy tree species (Engone Obiang et al., 2019). An airborne lidar campaign over 900 ha was carried in 2015, using a helicopter-based RIEGL VQ-480i, with pulse densities of ~2.5 per m^2, and the plot is part of the AfriSAR campaign (Fatoyinbo et al., 2017).

2.2 The Canopy Constructor algorithm

The Canopy Constructor algorithm consists of two steps. In a first step, the 3D-forest structure is reconstructed over a local plot ("calibration plot"), relying on a tree inventory, a co-registered ALS-scan and stand-average allometric relationships that relate trunk diameter, tree height and crown radius. After an initial, random reconstruction, tree properties are swapped until a high degree of similarity between the empirical, ALS-derived canopy and the simulated canopy is achieved, but without altering the underlying allometric structure. If allometric parameters are not known

empirically, they are inferred through Bayesian inversion where the routine is run with a wide range of parameters (see e.g., Hartig *et al.*, 2011). At the end this step, several best-fit 3D scenes are obtained, representing the most likely structural configurations and allometric scaling relationships on the calibration plot.

In a second step, the routine is extended to create a tree-by-tree reconstruction over the whole extent of the airborne lidar scan. Trees are drawn from the local stem diameter probability distribution and crowns are packed into the canopy until densities match those of the calibration plot. In the following, we describe both steps in detail.

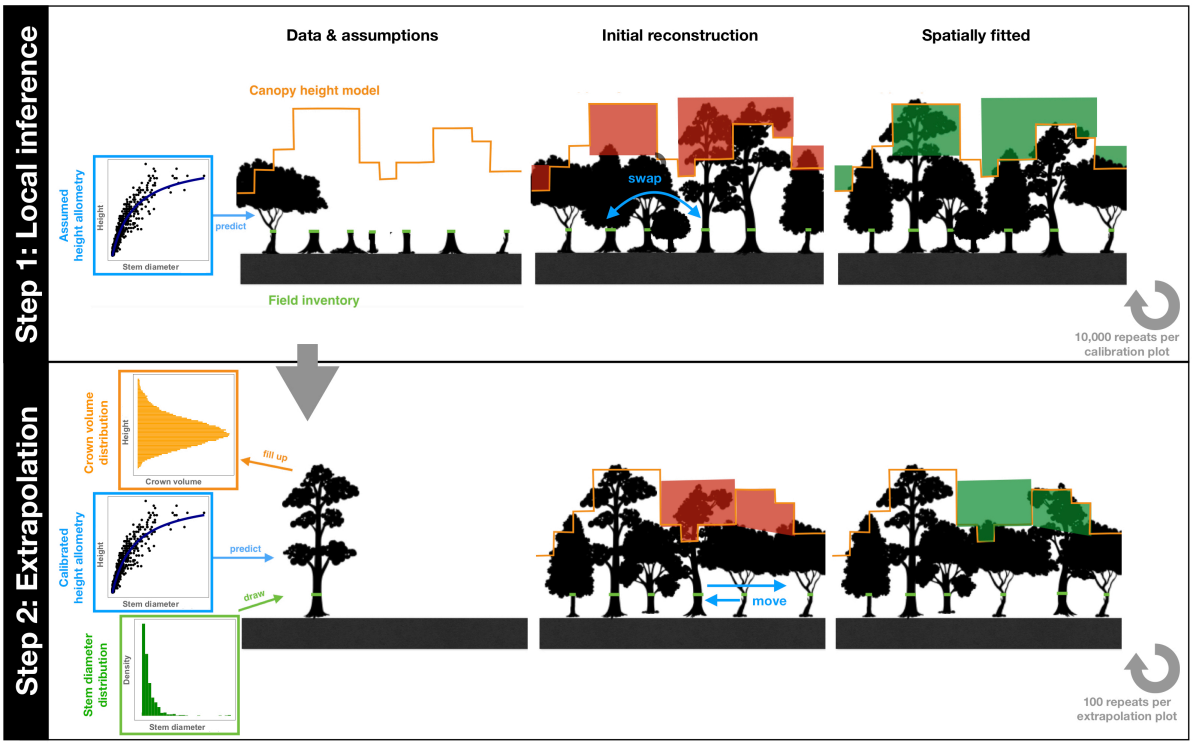

Figure 1: The two-step procedure of the Canopy Constructor algorithm. Step 1 uses tree inventory data, and a canopy height model (CHM). To infer the position and size of each tree, the algorithm creates an initial reconstruction drawing randomly dimensions from allometric relationships between tree dimensions. In ill-fitting regions (red), deviations from the allometric means are swapped between trees until a good spatial fit is obtained (green). Step 2 extrapolates the results of step 1 and creates virtual inventories across thousands of hectares, following the same fitting algorithm as in step 1, but with fitted trees drawn from a distribution (see main text for details).

The code was developed in C++ and is available online (https://github.com/fischer-fjd/CanopyConstructor). Statistical analysis and visualization were carried out in R (R Development Core Team, 2019) with the packages *data.table*, *raster*, *ggplot2*, and *viridis* (Dowle and Srinivasan, 2018; Garnier, 2018; Hijmans, 2016; Wickham, 2011) and their dependencies.

2.2.1 Forest structure inference and model calibration

The Canopy Constructor inputs tree diameters and locations from a forest inventory, predicts tree heights and crown diameters from allometric scaling and fills up an initial 3D-canopy for the fitting procedure (resolution of $1m^3$), as in the TROLL model (Maréchaux and Chave, 2017). To summarize canopy structure, we chose the canopy height model (CHM), defined as the top-of-canopy height above ground for a given grid cell (here at $1m^2$ resolution). For the tree-by-tree reconstruction, the minimal trunk diameter size was set to 1 cm. Each surveyed tree was assigned to a grid with $1m^2$ cell size. If several trees co-occured on the same cell, their positions were slightly jittered to fill up adjacent cells. For multistemmed trees, a single effective stem dbh was retained, equal to $dbh_{eff} = \sqrt{\sum_i dbh_i^2}$. For simplicity, we refer to dbh_{eff} as dbh. For tree inventories with a higher cutoff than 1 cm (e.g. dbh_{cutoff} = 10cm or 30cm), power-law and exponential dbh-size distributions were assumed to fill up and randomly place trees < dbh_{cutoff} (Taubert *et al.*, 2015, Farrior et al., 2018).

Allometric relationships

To predict canopy structure from the field-measured stems, the Canopy Constructor assumes the following allometric models:

$$h = \frac{hmax \times dbh}{(a_h + dbh)} \times \exp(\varepsilon_h) \quad (1)$$

and

$$cr = \exp(a_{cr} + \varepsilon_{cr}) \times dbh^{b_{cr}} \quad (2)$$

In Equation (1), h is total tree height, dbh diameter at breast height, while $hmax$ and a_h are Michaelis Menten coefficients interpreted as the asymptotic height that trees reach at large trunk diameter values and the approximately linear slope of the increase of height with diameter at small trunk diameters, respectively. In Equation (2), cr is the tree's crown radius, and a_{cr} and b_{cr} are the intercept and slope of a log-log regression, i.e. a power law model. Equation (1) was chosen instead of a power model to better capture the saturating relationships typically found in tropical rain forests (Cano et al., 2019). The ε_h and ε_{cr} are the respective error terms – i.e. the natural variation in allometry –, given by:

$$\varepsilon_h \sim N(0, \sigma_h) \quad (3)$$

and

$$\varepsilon_{cr} \sim N(0, \sigma_{cr}) \quad (4)$$

The error terms generate a multiplicative error structure that accounts for the heteroscedasticity in crown and height allometries (Molto et al., 2014). We assumed that allometric variation did not depend on species identity, that ε_h and ε_{cr} were independent, and that crown depth could be simply calculated as a proportion of h, as in the TROLL model (Maréchaux and Chave, 2017).

To model crown shape more realistically, we defined the ratio γ between the radius at the top of the crown and its base, with a linear slope linking both layers. γ varies between 0 and 1: if $\gamma = 0$, the tree crown is a cone, while if $\gamma = 1$, it is a cylinder (as in Maréchaux & Chave, 2017). For the purposes of this study, we set γ to 0.8. This

resulted in an improvement in the convergence of the crown fitting algorithm compared to simpler cylindrical shapes, better modelled the less clear-cut edges found empirically and accounted for the fact that real tree crowns are smaller than their cylindrical envelopes.

Based on the crown shape parameter as well as a particular realization of the six allometric parameters ($hmax$, a_h, a_{cr}, b_{cr}, $\varepsilon_{h,}$ ε_{cr}), we created an initial 3D forest mockup, with deviations from allometric means randomly assigned to trees.

Optimization algorithm

The Canopy Constructor then optimizes the spatial overlap of the simulated and the ALS-derived CHMs by readjusting trees and their crowns in space. To this effect, we looped repeatedly through all trees on the grid, in random order, and applied one of three operations described below. The loop was stopped when improvements in canopy structure were marginal (< 1% acceptance rates), usually achieved after 100-200 iterations. A similar algorithm was implemented in Taubert *et al.* (2015).

For the majority of field-measured trees, we picked pairs of trees and swapped their respective values of ε_h (deviation in height) and ε_{cr} (deviation in crown radius). We then recalculated the new dimensions of both trees and kept the change if it resulted in an increase in the overall goodness of fit between the simulated and ALS-derived CHM. To keep the overall variance structure, trees were binned into logarithmic dbh classes and only swapped when they were in the same dbh class. This procedure rapidly redistributed deviations from the allometric means across the population of trees so as to improve spatial fits, but preserved the initial allometric structure.

We defined two exceptions. First, large tree crowns are crucial to obtain a good canopy reconstruction, but only have limited opportunities to swap dimensions due to

their low numbers. Therefore, if there were less than 10 trees within a dbh bin across the plot, we drew new tree sizes from equations (1) and (2). If the new draw resulted in a better fit to empirical data, it was retained. To prevent bias in the allometric structure, the expected crown radii and heights had to be preserved. We used a simple method, allowing positive deviations from the mean only if the previous bin average deviated negatively from the expected value, and vice versa.

Second, for trees with dbh < dbh_{cutoff}, initial positions were chosen at random, so we did not change the trees' dimensions, but instead relocated the entire tree, within a radius dependent on its height (but at least 10 m). If the new location increased the goodness of fit, the change was accepted. Few small trees were visible in the CHM, so this procedure rarely modified the canopy, except in canopy gaps.

Plot boundaries bisect crown areas and may thus introduce errors in estimation procedures (Mascaro *et al.*, 2011). To prevent biased estimates, we calculated the crown area outside the plot CA_i^{out} and the total crown area CA_i for each tree *i*, summed both across all n trees per plot and computed the ratio $R = \frac{\sum_{i=1}^{n} CA_i^{out}}{\sum_{i=1}^{n} CA_i}$. During the optimization procedure, we forced *R* to remain approximately constant. If during the fitting process, *R* exceeded its initial value, then the trial was accepted only if it lowered *R*, and vice versa.

We further observed that the Canopy Constructor could assign large crowns to lower canopy layers that barely affected the CHM and fit small crowns on the tallest trees to mimick natural heterogeneity, a phenomenon similar to oversegmentation in tree delineation approaches. To prevent this, we circled through all trees within a distance $dist = CR_{tree} + CR_{treemax}$, for every newly fitted crown with CR_{tree}, and rejected crown fittings that resulted in tree configurations where a large tree with a small crown pierced a small tree with a large crown.

300

301 ***Goodness-of-fit metrics***

302 Each time a tree crown was updated, we tested whether this change increased the fit
303 with empirical values. To assess the goodness of the fit between virtual and empirical
304 CHMs, we used the mean of the absolute errors:

$$MAE = \frac{1}{s_{total}} \sum_{s=1}^{s_{total}} \left| chm_{emp}(s) - chm_{sim}(s) \right| \quad (5)$$

305 where each *s* represents a 1m² grid cell of forest, chm_{emp} the empirical canopy height of
306 that grid cell, chm_{sim} the simulated canopy height, derived from the highest non-empty
307 voxel, and s_{total} the total number of grid cells within the plot. MAE measures the
308 matching of local canopy height patterns and was used instead of a mean squared error,
309 because it is more robust with regard to outliers (Hill and Holland, 1977).

310 Since initial tests showed that the size of large trees would be underestimated by
311 shrinkage towards the mean from an optimization of *MAE* alone, we also used the
312 dissimilarity index of the canopy height distributions:

$$D = \frac{1}{2} \sum_{h=0}^{h=hmax} \left| \mathrm{d_{emp}}(h) - \mathrm{d_{sim}}(h) \right| \quad (6)$$

313 where *h* is a discrete height index (in m), and $\mathrm{d_{emp}}$ and $\mathrm{d_{sim}}$ are the densities of the
314 empirical and simulated height histograms across the surveyed area, i.e. total number of
315 canopy height occurrences, normalized by the number of 1m² grid cells. The factor ½
316 normalizes the metric to 1 and allows us to interpret it as a measure of distribution
317 overlap: the lower the dissimilarity, the higher the overlap. In the limit of $D = 0$, both
318 distributions are identical, in the limit of D = 1, there is no overlap at all. Formally, if *OVL*
319 is the distribution overlap, then $D = 1 - OVL$, with $OVL = \sum_{h=0}^{hmax} \min \left(d_{emp}(h), d_{sim}(h) \right)$
320 (Inman and Bradley, 1989; Swain and Ballard, 1991).

We fitted the tree crowns using both metrics independently first, until a low acceptance rate was achieved for each (< 1% for trees > 10cm dbh, typically reached within 50 iterations for the *MAE*, and within 5 iterations for the dissimilarity). We then used the difference between initial and final fits to normalize both metrics and combined the normalized values to an overall error as follows:

$$\delta = \sqrt{MAE_{norm}^2 + D_{norm}^2} \quad (7)$$

In a final number of iterations, we minimized δ. The combined metric ensured that crowns did not only fit spatially at local scales, encapsulated by a low *MAE*, but also preserved the overall canopy height model distribution, as measured by *D*.

Inferring Allometric Parameters by Approximate Bayesian Computation

The optimization algorithm finds the best canopy reconstruction, given a set of allometric parameters. However, allometric parameters are rarely known, so we used an Approximate Bayesian Computation rejection scheme (Csilléry *et al.*, 2010; Hartig *et al.*, 2014; F. J. Fischer *et al.*, 2019) to infer them. The prior probability distribution of the six allometric parameters, ($hmax$, a_h, a_{cr}, b_{cr}) and (σ_h, σ_{cr}) was approximated by 10,000 random draws. We applied the Canopy Constructor to the allometric parameter combinations, and retained only the best 1% of canopy reconstructions (Csilléry et al., 2010). The retained parameter values were used to generate a posterior probability distribution over credible allometric parameterizations given the data.

We chose flat parameter priors by drawing from uniform distributions within globally observed ranges of tree allometries (Jucker et al., 2017). Parameters were drawn on logscales, except for the crown allometry intercept a_{cr}, drawn from a uniform distribution on the back-transformed scale. A Latin hypercube scheme was employed to minimize the computational burden, and correlation between allometric coefficients

was accounted for using an algorithm of the R package 'pse' (Chalom et al., 2013), rewritten in C++ for speed. Covariance coefficients were taken from the Jucker *et al.* data set (2017). Since crown depth did not influence canopy height – and thus did not directly affect the fitting procedure –, it was fixed to 20% of tree height throughout the procedure.

To assess goodness of fit, we again used the mean absolute error (MAE) and dissimilarity D. But instead of normalizing by the within-simulation range, we normalized by the range across all simulations and combined the metrics to $\delta_{ABC} = \sqrt{MAE_{normABC}^2 + D_{normABC}^2}$.

2.2.2 Model extrapolation

In step 2, the Canopy Constructor uses the local fit from step 1, extrapolates the trunk diameter probability distribution and allometric scaling relationships across the whole ALS-covered area and constructs virtual tree inventories from space-filling principles. We implemented the same fitting procedure as before, but since the location and size of stem diameters have to be inferred, now all trees are drawn from a distribution and then relocated to create better spatial fits.

Space-filling principles

As a measure of space-filling, we used the crown packing density $\varphi = \frac{1}{V_{max}} \sum_i V_i$, where V_{max} is the maximally available volume within a section of the canopy, and V_i the volume contribution of each tree to that section (Jucker et al., 2015; Taubert et al., 2015). The crown packing density is the ratio of unit crown volume to unit canopy volume (m^3 per m^3). It can be calculated for single voxels, subsets of voxels or for the entire canopy.

We defined the crown packing density at height h, with $0 \leq h \leq h_{max}$, and with h_{max} top-of-canopy height, so that crown packing density was dependent on the canopy's height. We then defined the following quantity: $\boldsymbol{\varphi}(h, h_{max})$, the packing density matrix, where columns represent top-of-canopy height h_{max} and rows represent within-canopy height layers h (cf. Figure S2, left panel). We set the size of height bins to 1 m, and their numbers ran from 0 m to maximum canopy height. On a per-voxel basis, each tree's volume contribution to a voxel could thus be either 0 or 1 m^3, but due to the idealized crown shapes assumed in the Canopy Constructor, crown overlaps were more frequent than in real forest stands, resulting in local packing densities > 1 m^3.

Inferring virtual inventories

To infer virtual tree inventories across the whole ALS-covered area, we divided the lidar scene into grid cells, roughly equivalent in size to the local field inventories. We then used the CHM of each grid cell, combined it with the packing density matrix $\boldsymbol{\varphi}$ obtained from the 3D reconstructions of the local calibration plot and predicted crown volume per height layer. This was achieved by calculating the ALS-derived canopy height distribution for each grid cell, denoted $\bar{c}_{ALS}$, and formalized as a vector of top-of-canopy height frequencies. Multiplying the ALS-derived canopy height vector with the packing density matrix yielded the vector $\bar{v}_{ALS} = \boldsymbol{\varphi}\bar{c}_{ALS}$ (Figure S2). The quantity $\bar{v}_{ALS}$ is an estimate of total crown volume per height layer within the extrapolation cell. For grid cells that reached canopy heights larger than the calibration plot from which the packing density matrix was derived, $\boldsymbol{\varphi}$ was calculated by averaging over the five non-empty layers just beneath the missing layer.

Once the maximum space filling was determined, trees were drawn until a virtual forest with a crown volume distribution $\bar{v}_{virtual}$ similar to $\bar{v}_{ALS}$ was obtained. We drew

diameters from the calibration plot's probability distribution and used the previously inferred allometric relationships to predict tree height and crown radius. After randomly placing a tree on the grid, we updated $\bar{v}_{virtual}$ and determined by how much the new tree improved the fit with $\bar{v}_{ALS}$. To do so, we calculated the change in $\bar{v}_{diff}(h) = \bar{v}_{ALS}(h) - \bar{v}_{virtual}(h)$ for every height layer *h*. If the crown volume in *h* had not yet reached the reference value ($\bar{v}_{diff}(h) > 0$), every added unit of crown volume improved the fit and was counted positively. As soon as the crown volume in the layer reached or exceeded the ALS-predicted volume ($\bar{v}_{diff}(h) \leq 0$), every added crown volume unit penalized the fit and was thus discounted. We then summed units of crown volume over all layers *h*, and we accepted the tree if the overall balance was positive. Otherwise, the tree was rejected. Each drawing cycle comprised *n* draws, where *n* is the number of potential tree locations (i.e. the m^2 area) under consideration. When the rejection rate reached 100% after a full cycle, we stopped the procedure.

After the initial distribution of trees in space was obtained, it was gradually improved upon. This was done by displacing trees in relation to their height until an optimal spatial fit was achieved, as described for step 1. Again, we found that 100-200 iterations were sufficient to reach low rejection rates (< 1%). To propagate uncertainty, the procedure was carried out for each of the 100 posterior reconstruction of the ABC approach from step 1, with all grid cells collated to produce final maps.

2.2.3 Application at the study sites

At Nouragues, we used the geographically separated Petit Plateau (12 ha) and Grand Plateau (10 ha). Applying the inference step on each of them individually allowed for a comparison with previous studies and an assessment of within-site heterogeneity. We also split the 25-ha plot at Rabi into two subplots (10-ha and 15-ha, respectively). We

used plot sizes of ≥ 10ha because they minimized edge effects and kept a balance between the computational burden of the procedure and the sample sizes needed to swap random terms between crowns. On each subplot, we inferred forest structure (tree dimensions, allometric parameters and crown packing densities). We then used the larger plots at both sites (i.e. the 12 ha Petit Plateau and the 15 ha Rabi plot) to extrapolate the virtual inventories across the whole landscape, subdivided into 400m x 400m grid cells (16 ha). Grid cells at the edges were discarded, and we created virtual forest inventories over 2,016 ha at Nouragues and 832 ha at Rabi.

To create the CHMs, lidar data were classified via TerraScan and then post-processed with LAStools to obtain pit-free CHMs (Isenburg, 2018; Khosravipour et al., 2014). While the ALS data differed in point densities at the two sites (with considerably lower densities at Rabi), the Canopy Constructor method was robust to such differences because it was based on the CHM alone. Aboveground biomass (AGB) was estimated for each tree (kg), using the formula $AGB = 0.0673 \times (\rho \times dbh^2 \times h)^{0.976}$ (Chave et al., 2014), where ρ represents species-level wood density, obtained from a global database (Chave et al., 2009; Zanne et al., 2009). For biomass mapping, tree biomass estimates were aggreggated at 1 ha and 0.25 ha resolutions (t ha^{-1}), a common grid size in biomass mapping (Labrière et al., 2018; Réjou-Méchain et al., 2015). For consistency with previous work, we computed AGB only for trees with dbh ≥ 10cm. Diameter measurement errors usually have small effects on plot-scale estimates (Réjou-Méchain et al., 2017), and since neither ρ nor error in the AGB equation directly affected the Canopy Constructor algorithm, we did not propagate error in these quantities.

2.3 Evaluation

We assessed the accuracy of the Canopy Constructor's reconstructions (step 1) by comparing the inferred allometric relationships between trunk diameters and tree dimensions to allometric relationships derived from field measurements of tree height and diameter. We computed the mean absolute and mean relative deviation (in %) between height predictions. For biomass, we compared our predictions to previous estimates of plot biomass for both sites and landscape-scale maps obtained with a pooled regression model, all reported in Labriere et. al. (2018).

To more formally assess the extrapolation to landscape scale (step 2), we first evaluated the consistency of the extrapolation model with the reference estimate, derived from the field inventory and Canopy Constructor-calibrated allometries (step 1). We did so by applying the extrapolation step to each plot itself and assessed the fit of the extrapolation model. We quantified the accuracy and precision of biomass estimation via four commonly reported metrics, namely R^2 (squared Pearson's r), RMSE (root mean squared error, t ha^{-1}), MAE (mean absolute error, t ha^{-1}) and MBE (mean bias of the error, t ha^{-1}). All metrics, except R^2, were also computed relative to the reference AGB. We then evaluated the sensitivity to plot characteristics through a cross-validation procedure where we used the summary statistics from one plot per study site (calibration plot) to extrapolate to the other plot at the study site (extrapolation plot), and vice versa. As before, we quantified accuracy with respect to reference AGB estimates through R^2, RMSE, MAE and MBE. Finally, we also compared the reference and predicted diameter distributions, both for the model fit and in cross-validation.

To evaluate the Canopy Constructor's utility for biomass estimates compared to more conventional methods, we compared its accuracy to the accuracy of log-log

regression models of AGB vs. median canopy height (Labriere et al., 2018; Réjou-Méchain et al., 2015). We fitted log-log regression models against median canopy height, again for each of the four plots at both 1 ha and 0.25 ha resolution and assessed both model fit at the calibration plot and predictions between cross-validation plots. To mirror the Canopy Constructor setup, we did not use any field-inferred height allometries for the AGB estimates, but inferred height from a bioclimatic predictor (Chave et al., 2014; Réjou-Méchain et al., 2017). Accuracy was reported with the same metrics as above (R^2, RMSE, MAE, MBE).

Throughout this study, we carried out a comprehensive Bayesian inference with 10,000 prior and 100 posterior simulations. This gave a good approximation of the Canopy Constructor's posterior distributions, but, more importantly, also allowed us to assess the method's sensitivity to simulation numbers. To this effect, we resampled 100 sets of 1,000 simulations from the 10,000 prior simulations, and 100 sets of 10 simulations from the 100 posterior simulations, and repeated both steps of the Canopy Constructor to assess accuracy and precision in a computationally more efficient setting.

3. Results

3.1 Reconstructions of tropical forest canopies in 3D

Across all plots, the Canopy Constructor yielded good fits for the canopies with a final error in mean canopy height of 0.66m [95% credibility interval: -0.41, 1.8] or 2.7% of mean canopy height, and a mean absolute error of 3.98m [3.02, 4.98] or ~14.4% of mean canopy height. Figure 2 visualizes the approach at the Petit Plateau plot for a posterior simulation after 200 iterations of fitting. The initial draw (panel a) already mirrored average properties of the empirical canopy, but not the spatial location of its features (panel b). Swapping the deviations in allometries greatly improved the spatial structure (panel c).

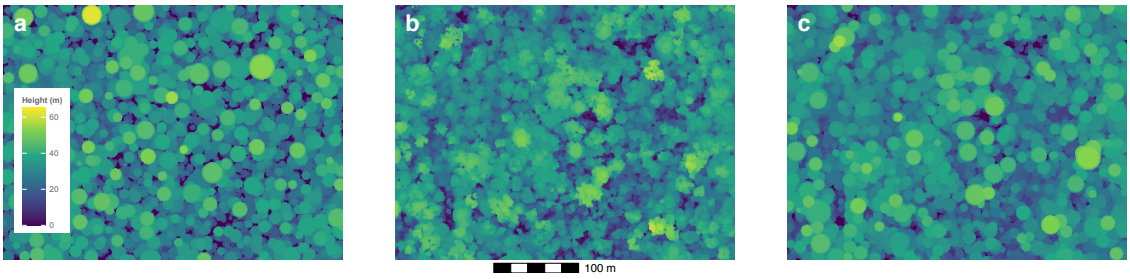

Figure 2: Example of canopy reconstruction at the Petit Plateau plot, Nouragues. Shown are the initial canopy height model (CHM) where tree dimensions are randomly drawn from site-specific allometries (a), the ALS-derived CHM (b), and the final reconstruction of the Canopy Constructor (c).

3.2 Allometric scaling relationships

Tree inventories and ALS data were sufficient to infer allometric relationships between tree dimensions at both sites. Across all plots, we found substantial covariation between allometric parameters (Table S1, and Figure S3, left panels), but height allometries had lower uncertainties than crown radius allometries (Figure 3, Figure S3, Table 1). High within-site similarity was found for height allometries at both Nouragues and Rabi (Figure 3). Crown allometries, on the other hand, showed a divergence at Nouragues,

with larger crown radii predicted at Petit Plateau than at Grand Plateau. The sites were clearly distinct in their height allometries, with generally taller trees at Nourages than at Rabi, but not in their crown allometries.

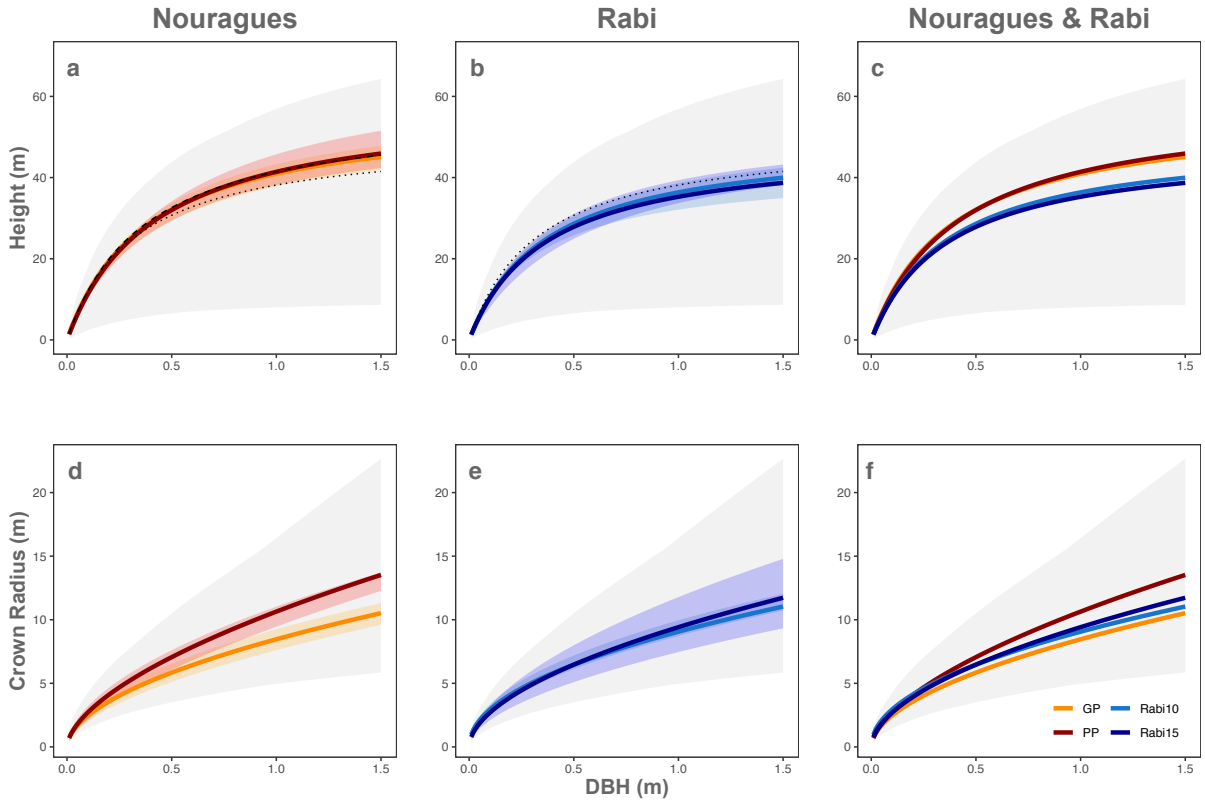

Figure 3: Inferred allometries at Nouragues and Rabi (step 1). The panels show height allometries (top row) and crown allometries (bottom row), as inferred by the Canopy Constructor, for Nouragues (a,d), Rabi (b,e) and both sites combined (c,f). The grey background indicates the prior range. Mean and 75% highest density intervals are given for each plot separately, i.e. for Grand Plateau (orange) and Petit Plateau (dark red) at Nouragues, and for the 10ha (light blue) and 15ha (dark blue) plot at Rabi. As comparison, we have plotted empirical height allometries measured from in the field for both Grand Plateau (dotted) and Petit Plateau (dashed) in the top panels, as well as a single ground-inferred allometry at Rabi (dotted). Results for same inference procedure, but with a lower number of simulation runs, are provided in Figure S8.

At both sites, parameter estimates were close to those previously obtained from field measurements of tree height (cf. Figure 3, top row). At Nouragues, the Canopy Constructor's height estimates were slightly lower than empirical ones at small diameters and exceeded them at large diameters, but mirrored their qualitative patterns, i.e. the larger heights predicted at Petit Plateau compared to Grand Plateau. The difference to empirical height predictions never exceeded 1m (or 2%) at Petit Plateau, versus 3.2 m (or 7.8%) at Grand Plateau. At Rabi, the pattern was inversed, with lower predictions of tree height at large diameters than from empirical data, but differences never exceeded 11% (Supplementary Figure S4).

Table 1: Inferred parameters. Mean of posterior distributions for allometric parameters at the two sites. Plots are Grand Plateau (GP) and Petit Plateau (PP) at Nouragues, and the 10 ha and 15 ha rectangular strips at Rabi (Rabi10 and Rabi15, respectively). a_h and h_{max} are given in m, all other variables are unitless.

	a_h	h_{max}	σ_h	a_{CR}	b_{CR}	σ_{CR}
GP	0.41	56.88	0.39	2.19	0.55	0.24
PP	0.39	58.38	0.23	2.29	0.56	0.22
Rabi10	0.32	47.52	0.37	2.2	0.53	0.25
Rabi15	0.28	43.67	0.35	2.23	0.55	0.27

3.3 Biomass mapping at landscape scale

Aboveground biomass was estimated to be 400.8 t ha^{-1} at the Nouragues plots [366.2 – 437.9] and 302.2 t ha^{-1} [267.8, 336.8] at Rabi. Within-site standard deviation at hectare scale was 105.1 t ha^{-1} [86.5, 120.7] at Nouragues and 71.0 t ha^{-1} [60.5, 83.6] at Rabi. At both sites, biomass density decreased at the landscape scale to an average of 299.8 t ha^{-1} [275.9, 333.9] and 251.8 t ha^{-1} [206.7, 291.7], respectively, but with considerable heterogeneity (Figure 4, a and d). Map uncertainty was highest at vegetation edges and low biomass areas, and generally higher at Rabi (median coefficient of variation of ~0.24) than at Nouragues (~0.16, cf. also Figure 4, b and e). At both Nouragues and Rabi,

aboveground biomass reached similar extreme values, of over 1100 t ha^{-1} at the 0.25-ha scale.

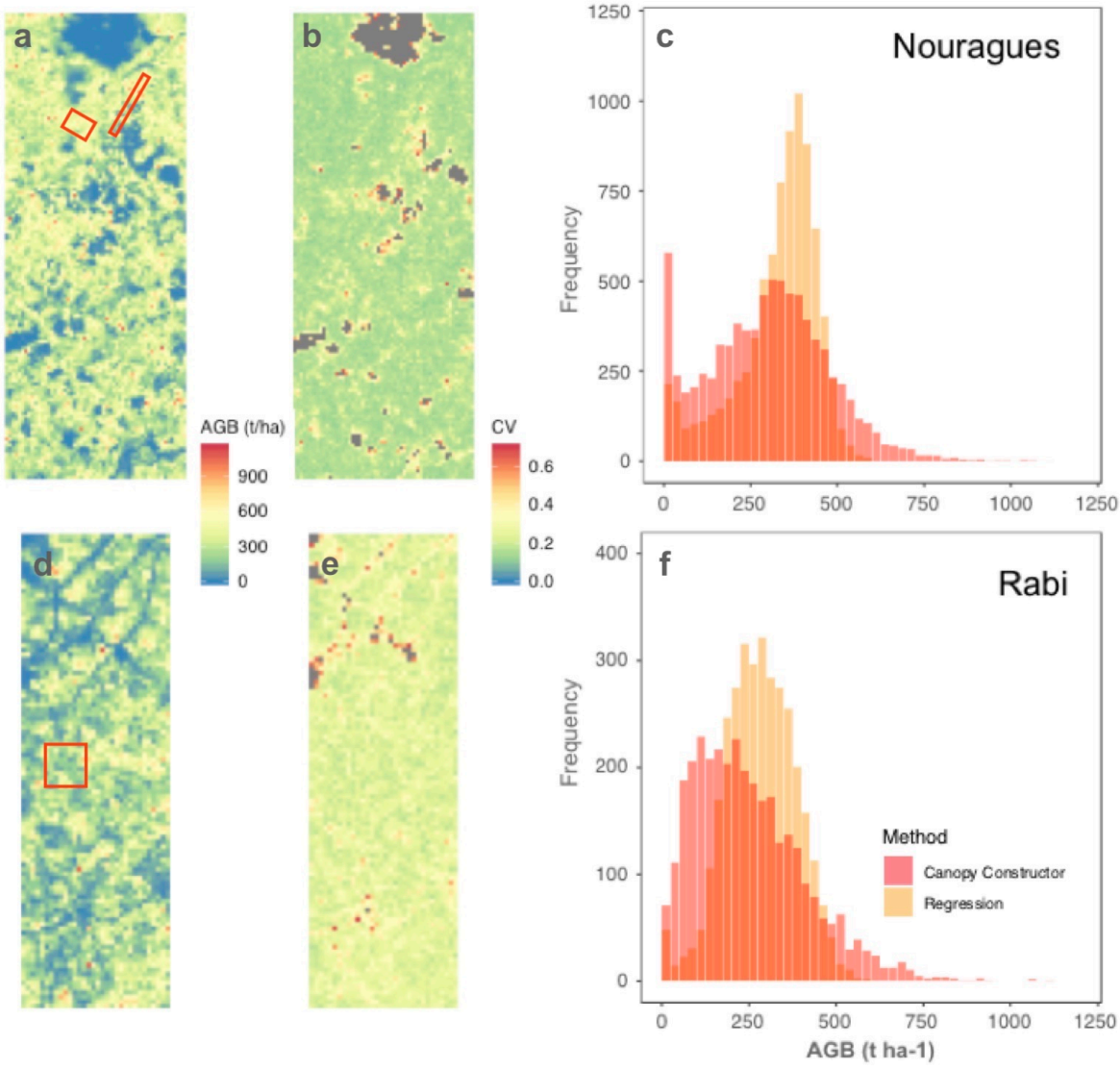

Figure 4: Aboveground biomass predictions for ALS campaign at Nouragues and Rabi (step 2). Maps show the mean aboveground biomass values (t ha^{-1}) predicted with the Canopy Constructor approach across 2,016 ha at Nouragues (panel a) and 832 ha at Rabi (panel d), as well as the respective coefficient of variation across 100 simulations (panels b and e, dimensionless). Also given are the overall distributions of aboveground biomass (panels c and f, red distributions, in t ha^{-1}) and previously obtained estimates (panels c and f, yellow) from a pooled regression-model (Labrière et al. 2018). Clearly evident is the shrinkage towards the mean in the regression-based approach, as opposed to much stronger variation in the Canopy Constructor approach. Please note that the geographic extent of the maps has been rescaled for visualization purposes.

Biomass estimates were close, but lower at both sites than previous estimates of 404.6 t ha-1 at the plot and 328.6 t ha^{-1} at landscape scale at Nouragues, and 314.6 t ha^{-1} 282 t ha-1 at Rabi (Labriere et al., 2018). However, the spread in aboveground biomass density was much larger than in previous biomass maps, with a larger fraction of both low- and high-density grid cells (Figure 4, c and f).

3.4 Extrapolation accuracy

Across both sites, the extrapolation model's biomass predictions were consistent with the locally inferred reference values (Figure 5, a and c), with an R^2 of 0.84 at the 1 ha scale, and 0.67 at the 0.25 ha scale. The RMSEs were 53.2 t ha^{-1} (14.7%) and 87.3 t ha^{-1} (24.1%). The calibration plots were also representative of the local environment, as the quality of the inference did not decrease in cross-validation, with identical R^2 values and similar RMSE as before, i.e. 53.7 t ha^{1} at the one-hectare scale, and 87.6 at the 0.25 ha scale, or 14.9% and 24.2%, respectively (Figure 5, b and d). The good predictive accuracy was mirrored by diameter distributions that matched well empirical ones, both when fit at the calibration site and in cross-validation (Figures S5 and S6, Table S2).

Regression-based approaches generally produced better model fits at the calibration sites than the Canopy Constructor, but there was no clear advantage in cross-validation, with R^2 = 0.72 at the 1 ha scale and 0.55 at the 0.25 ha scale, and an RMSE of 51.6 t ha^{-1} (14.6%) and 81.4 t ha^{-1} (18.3%), respectively (Figure S7). Bias was slightly higher in the Canopy Constructor, at -4.7%, compared to a +1.2% in regression, but the Canopy Constructor predicted much larger heterogeneity than the regression-based approach. In the calibration step, it had a 95% range in AGB of 489.7 t ha^{-1}, compared to 458.5 t ha^{-1} at the 0.25 ha scale, and the difference was even larger in extrapolation, with a predicted range of 568 t ha^{-1} against 368.3 t ha^{-1} from regression (54% increase).

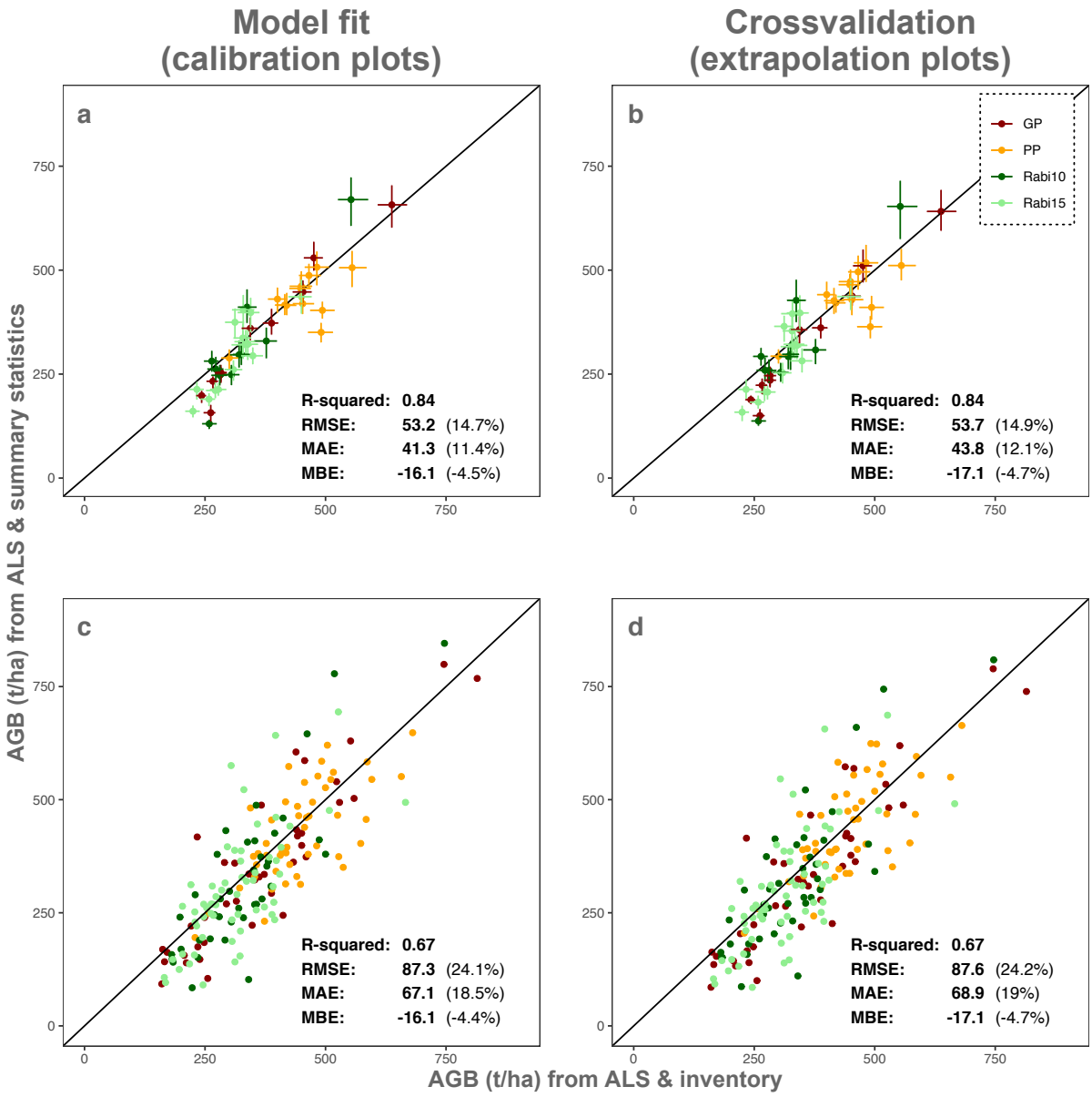

Figure 5: Evaluation of aboveground biomass predictions in extrapolation (step 2). Shown are the predictions of aboveground biomass (median of 100 posterior simulations, given in t ha^{-1}) at the 1 ha scale (a, b) and 0.25 ha scale (c, d). The left column shows the results when the space-filling approach is applied at the calibration plot from which allometries and packing densities were derived ("Model fit"), the right column the results when the approach is transferred between plots ("Cross- validation"). The Nouragues results are plotted in red/orange, and for Rabi in dark/light green. Goodness of fit values are provided in the bottom-right corner of the panels. MBE does not change between 0.25 and 1 ha scales and is thus only given in the top panels. For visualization purposes, we only plot error bars at the hectare scale, representing the interquartile ranges of estimates from 100 posterior simulations.

All our estimates were stable and had low uncertainties when resampling smaller sets of simulations. Within plots, height allometric parameters were similar to the full simulation set (example inference in Figure S8). Average AGB was also similar to the full simulation set, with 399.2 t ha^{-1} at Nouragues and 305.0 t ha^{-1} at Rabi, and small standard deviations of 5.7 t ha^{-1} (1.4%) and 5.6 t ha^{-1} (1.8%). The average R^2 in extrapolation was 0.65 at the 0.25 ha scale with an average RMSE of 90.7 t ha^{-1}, and standard deviations of 0.02 and 2.8 ha^{-1}, respectively (or ~3% for both metrics).

4. Discussion

We described and applied a new approach to quantifying forest structure, the Canopy Constructor. The Canopy Constructor inputs local forest tree inventories and airborne lidar scanning and outputs estimates of forest structure, allometric relationships among tree dimensions and virtual landscape-scale tree inventories. These results provide insights on tree allometric relationships and the distribution of carbon stocks. Below we discuss how the method advances our knowledge on both issues, and we reflect on the underlying assumptions and computational limitations. We applied our approach at two tropical forest sites, one in the Guiana Shield of South America, the other in the Guineo-Congolian rainforest of Africa. We selected the two sites because they are geographically and floristically distinct, but represent high-carbon stock forests, those for which classic airborne lidar scanning (ALS) methods of biomass mapping are the most error prone. We also discuss whether the Canopy Constructor method is applicable beyond closed-canopy tropical forests, e.g., in landscapes with land-use mosaics, and in temperate and boreal forests.

Inferring allometric relations in forest trees

We used the first step of the Canopy Constructor in a Bayesian setting to infer the allometric relationships between tree height and trunk diameter (dbh), and between crown size and dbh. Such allometric relationships are essential for scaling up from individual trees to forest canopies, and we found that they could be well-inferred from a combination of field inventories and ALS data alone.

In particular, we found that height-diameter relationships differed more strongly between than within sites, suggesting that biogeographic constraints at the macroscale outweighed micro-environmental effects, such as disturbances, in shaping the two

624 forests' height scaling relationships. Crown radius allometries, on the other hand, had
625 higher uncertainties and were not clearly separated between sites. However, the French
626 Guiana plots displayed considerable within-site differences in their crown radius
627 allometry. While trees generally show both plasticity in height growth and the lateral
628 extension of the crown (Henry and Aarssen, 1999, Jucker et al., 2015; Pretzsch and
629 Dieler, 2012), height growth is also strongly influenced by physiological limitations
630 (Niklas, 2007). Horizontal crown growth, on the other hand, may depend strongly on
631 canopy openings, particularly so for mid-sized canopy trees, which might explain why
632 we recorded such a notable difference at the Nouragues site, where the two plots have
633 very different disturbance regimes.
634 One key assumption of our approach is that a single functional form holds across
635 a wide range of environmental conditions, forest cover types and functional groups.
636 Specifically, equations (1) and (2) assume a Michaelis Menten model for the dbh-height
637 relationship, and a power-law model for the dbh-crown size relationship, and we make
638 the strong assumption that variation in tree architecture can be summarized by
639 variation in six pre-defined allometric parameters ($h_{max}, a_h, \sigma_h, a_{cr}, b_{cr}, \sigma_{cr}$). On the one
640 hand, there is considerable empirical evidence for global scaling relationhips between
641 plant dimensions (Jucker et al., 2017), and there are strong theoretical arguments for
642 their generality due to constraints on resource uptake and hydraulics (West et al., 1999;
643 Niklas, 1994; Niklas, 2007). On the other hand, physiological constraints depend on
644 climatic conditions and are shaped by the organisms' evolutionary history and
645 ecological niches (Niklas, 1994), so allometric relationships vary strongly across
646 environments, among species and co-vary with growth strategies and plant functional
647 traits (Cano et al., 2019; Lines et al., 2012). Empirical data also show deviations from
648 idealized allometric relationships due to disturbances and size-dependent competition

among plants (Coomes et al., 2003). In light of this knowledge, there is currently not enough evidence that equations (1) and (2) are valid across all of the world's forest types. However, they are flexible enough to accommodate a wide range of tree forms and have been previously found to yield good fits at our study sites and for other tropical rain forests (Labriere et al., 2018; Feldpausch, et. al. 2012).

In tropical forests, in particular, the Michaelis-Menten functional form has been shown to well-represent the saturating scaling relationships between diameter and tree height (Molto et al., 2014, Cano et al., 2019) and is commonly used to improve biomass estimates (Feldpausch et al., 2012, Réjou-Méchain et al., 2017). However, field data on tree height are difficult to obtain, so the number of empirically derived dbh-height allometric models remains limited in the tropics (Sullivan et al., 2018). The retrieval of crown radius is equally, if not more challenging in dense canopies. The Canopy Constructor approach circumvents such data acquisition problems by parameterizing the scaling relationships directly from a combination of geo-located trunk diameters and ALS-derived canopy height models. At both our study sites, in French Guiana and Gabon, the approach considerably narrowed down the parameter ranges for the inference of dbh-height tree allometries and dbh-crown radius allometries. Independent field data for the dbh-height allometry further confirmed that our inference matched the relationships derived from empirical measurements. The Canopy Constructor thus provides an important approach to estimate tree crown dimensions and biomass estimates where field measurements are scarce.

The allometric models described in equations (1) and (2) account for inter-individual variation in allometry through the parameters σ_h, σ_{cr}. For each allometry, a single terms is thus used to model variation due to life histories (King, 1996), species differences (Poorter et al., 2006; Thomas, 1996), and environmental conditions (Lines et

al., 2012). If allometries were inferred for different species or different functional groups, much lower variation around allometric means would be expected, with a probable reduction in uncertainty and more accurate representation of the underlying ecological relationships (Cano et al., 2019). However, there is also a tradeoff between increasing the number of model parameters to reduce uncertainty, and overfitting the model. Another risk is that few forest types currently have the level of information to implement species-specific versions of equations (1) and (2). In tropical forests, for example, there would likely not be enough field measurements to infer allometric relationships for rare species, and data might have to be pooled except for the most abundant species.

Recently, a wealth of information about tree allometry has been made available by the lidar scanning of entire trees from the ground (Dassot et al., 2011). Terrestrial lidar scanning (TLS) has reached a stage of maturity where it can now be applied to mixed-species forests, and even to all canopy trees from a stand (Calders et al., 2015; Momo Takoudjou et al., 2017; Newnham et al., 2015; Stovall et al., 2018). Furthermore, it allows the implementation of detailed canopy space-filling models (Pretzsch, 2014) and creates high-resolution renditions of the 3D architecture of individual trees. This novel source of information poses great challenges at the analysis stage (Åkerblom et al., 2017), but has become the best approach to test the generality of allometric exponents (Lau et al., 2019). In the future, it would be possible to either directly integrate TLS information into the Canopy Constructor at the parameter estimation stage (step 1), e.g. as an additional constraint on how the 3D voxel volume is filled, or to test the validity of the inferred scaling relationships.

This could be of particular value in heavily disturbed landscapes with few trees, where the simulation approach and its idealized crown shapes may fail to capture inter-

individual variation in tree architecture. However, it would likely have the strongest benefits for small understory species that are mostly hidden from the Canopy Constructor's fitting procedure. The latter do not only increase the range of allometries that fit the local forest plot and thus contribute strongly to the uncertainty in allometric inference, but they also increase the computational burden without considerably improving the 3D-fits . Nevertheless, it is vital to include small trees in our approach, since they reduce the bias in allometric estimates. Without them, the algorithm would extend crowns from the understory into gaps to improve the fit of the canopy height model and both underestimate tree heights and overestimate crown radii.

An alternative to the Canopy Constructor approach is to search for individual crown features by tree crown segmentation of ALS point clouds (Aubry-Kientz et al., 2019; Dalponte and Coomes, 2016; Ferraz et al., 2016) and to mtach the crowns to stems on the ground. In the future, a merging of both techniques could prove interesting: the Canopy Constructor algorithm has advantages for forest canopies where individual trees cannot be easily segmented, while individual tree crown segmentation methods are effective for emergent trees and more open forest landscapes. One option would be to first isolate easily identifiable trees, and then pass information on crown shape and size on to the Canopy Constructor. This would narrow down priors on allometric parameters and provide tie-points for the spatial fitting procedure.

Another important objective would be the improvement of the inference of crown radii, which showed higher uncertainty than inferred tree heights. So far, we did not impose any restrictions on crown overlap. This is at odds with observations (Goudie *et al.*, 2009) and may have increased the uncertainty, since crowns can be hidden within each other. A solution could be the simulation of phototropism and plasticity (Purves et al., 2008; Strigul et al., 2008), or the incorporation of leaf-level constraints, e.g. a

condition that assimilated carbon should be greater than respiration losses, as in the TROLL model (Maréchaux and Chave, 2017). We hypothesize that this would restrict the range of crown sizes, particularly in the understory where light limits tree growth.

Virtual forest inventories and carbon mapping

In the second step of the Canopy Constructor, the locally calibrated models are used to generate large-scale virtual tree inventories across thousands of hectares covered by ALS. We tested this approach at the two study sites and validated its performance through cross-validation. One of the main applications for these virtual tree inventories is the evaluation of carbon mitigation and conservation strategies.

Forest biomass is concentrated in a small number of large trees (Bastin et al., 2015; Lutz et al., 2018; Meyer et al., 2018), and mapping the spatial distribution of these trees is key to achieving high-resolution biomass estimates. Using ALS-data to extrapolate virtual inventories, the Canopy Constructor showed good predictive accuracy, mirroring well empirical tree densities and their biomass heterogeneity (Figure 4). The extrapolation uncertainty did not increase between the calibration and cross-validation plots. We validated this at Nouragues, where the plots have different disturbance regimes and different canopy height distributions (Figure S1). This suggests that the Canopy Constructor is an efficient method to map aboveground biomass across an entire landscape.

Specifically, the Canopy Constructor led to an improved biomass inference compared to regression-based approaches. Regression-based approaches, also known as area-based approaches (Coomes et al., 2017), infer mean stand biomass from ALS-derived canopy features, such as mean or median canopy height (Asner and Mascaro, 2014; Næsset, 2002; Zolkos et al., 2013). However, all regression-based inferences tend

749 to shrink the extreme values to the mean when uncertainty in the predicted variable is
750 not propagated or when there is strong variation in the independent variable, a
751 phenomenon sometimes called "dilution" bias (Réjou-Méchain et al., 2014). Because the
752 Canopy Constructor factors in the influence of large trees and makes use of the whole
753 canopy height model, we expected that it would mitigate this issue.

754 Indeed, we found a similar predictive accuracy for both methods, but the Canopy
755 Constructor better represented the heterogeneity of the canopy. The 95% range of
756 biomass estimates at the 0.25 ha scale was higher across both Canopy Constructor steps,
757 with an overall increase of 54% compared to an equivalent regression procedure.
758 Particularly noticeable were low biomass estimates for low-canopy forests that led to an
759 overall decrease in landscape-wide estimates at both Nouragues and Rabi compared to
760 previous biomass maps (Figure 4). Since many field inventories in the tropics are
761 established within primary forest, regression-based estimates are often calibrated on
762 tall canopies, and while additional field data would be required to validate this claim, it
763 may be that our individual-based approach better captures forest structure outside the
764 regression model's calibration range. Similarly, it likely better accounts for the large
765 multiplicative errors in tall canopies. Such fine-scale structural representations are
766 particularly important in identifying high-priority areas for carbon mitigation and
767 conservation, and when monitoring the impact of human interventions such as selective
768 logging on ecosystem functioning and animal habitats.

769 Furthermore, we hypothesize that there is considerable room for improvement of
770 future canopy reconstructions, since additional considerations on crown overlapping
771 and carbon balance or species' ecological strategies would likely improve the spatial
772 positioning of trees. The Canopy Constructor thus has the potential to be more widely
773 applicable across biomes and environmental conditions than currently used individual-

or area-based models (Coomes et al., 2017) and could provide an efficient means to assimilate forest inventories and ALS surveys into high-resolution aboveground biomass maps for the validation of remote-sensing biomass missions (Duncanson et al., 2019; Le Toan et al., 2011).

Nevertheless, the accuracy of biomass predictions with the Canopy Constructor also depends on the quality and the representativeness of the calibration sites.

First, while we do not assume that stem diameter probability distributions are identical across the whole area, we assume that they are similar enough to sample the entire diameter range. Ideally, they should not considerably over- or underrepresent a particular size-class. When the calibration plot covers a sufficiently large area (≥ 10 ha), microenvironmental features are likely well-sampled, and the space-filling approach of the Canopy Constructor will mostly compensate for deviations. However, in more heterogeneous landscapes than the ones selected for this study, it is essential to ensure that calibration plots are representative of all vegetation types.

Second, we assume that the vertical distribution of crown packing density within the canopy, as described by the local packing density matrix, is representative of the whole lidar-covered area. This crown packing matrix provides within-canopy densities conditional on top-of-canopy height and thus reflects disturbance regimes visible in the canopy height distribution. At the study sites, we found that a 10-ha forest inventory was sufficient to provide robust estimates of biomass even if the plot was not representative of the sampled area, as shown in the Nouragues forest. So, even if more studies are needed to fully explore this issue, we conclude that the assumptions of the Canopy Constructor do not lead to serious bias in biomass mapping as long as the sampled area is large.

Third, we extrapolate locally fitted allometries between tree dimensions across the entire landscape. This raises the question of whether an allometric model is valid beyond the stand where it was generated. Recently Jucker et al. (2017) have explored the generality of allometric relationships, with the aim to inform the link between field inventories and remote sensing. Compilation of empirical evidence suggests that some allometric relationships among tree dimensions are applicable outside of the locality where they have been constructed, but this may, again, need to be qualified if there is strong regional environmental variation or shifts in species composition (Beirne et al., 2019, Lines et al., 2012). Provided that enough data were available, separate allometric relationships for functional or species groups, likely more conserved across the landscape, could alleviate this problem in the future.

One of the main issues in extrapolation are understory trees, as they do not show up in the canopy height model and thus exclusively depend on the diameter distributions and crown packing densities of the calibration plots. The assumption of similar understory tree densities may be violated, for example due to browser pressure (Anderson-Teixeira et al., 2015b) or when the forest is more or less fragmented than at the calibration sites (Laurance et al., 2006). While the effect on biomass will be comparatively weak, understory densities can have important consequences for ecological dynamics, such as regrowth and resilience.

Here, we only had two calibration plots per site and they where either immediately adjacent (Rabi) or geographically close to each other (Nouragues), so the effect of spatial auto-correlation across the landscape could not be fully assessed. Any changes in soil characteristics, topography and floristic composition that may generate bias in our biomass maps, would, however, also affect regression-based approaches and can only be solved by more accurate sampling (Babcock et al., 2015; Spriggs et al., 2019).

Since most forest sites around the world involve small plots (0.25 ha or 1 ha) that are spread out in space to sample heterogeneous environments, a future evaluation of the Canopy Constructor's assumptions across forest types should not pose a problem.

Applicability across forest types and processing considerations

Many sites worldwide offer a combination of high-quality local forest inventories and ALS surveys (Duncanson et al., 2019), but far fewer provide quantitative information on the vertical arrangement of individual trees and within-canopy forest structure, so the Canopy Constructor was designed to be as widely applicable as possible. It only requires a canopy height model that covers the sampling area and a sufficiently large number of stem diameter measurements to accurately sample the diameter distribution. These conditions are likely already met within a few hectares in closed-canopy forests, and our results at two tropical forest stands provide evidence for this hypothesis.

The Canopy Constructor should, however, also be applicable to temperate and boreal forests, or more open landscapes, such as woodlands, savannas or heavily disturbed forests. Variable crown shapes can be accomodated through a crown shape parameter, ranging from cylindric to conic forms, and non-measured trees below a stem diameter cutoff can be supplemented by drawing from power-law or exponential functions, as done in the present study. Due to its simulation approach and need for representative calibration data, the Canopy Constructor reaches its limits in insufficiently or unequally sampled landscapes with low tree densities and strong floristic variation, but there, tree crown delineation would likely perform well and could complement it.

When applied across a wide range of forests, variation in wood density beyond the species level and variation in biomass allometries beyond a global mean would need

to be considered (Réjou-Méchain et al., 2017). This would likely further increase the local heterogeneity of simulated canopies, differentiate out between different successional stages and thus achieve a more realistic picture. However, since neither wood density nor biomass directly affect the Canopy Constructor procedure and since wood density is distributed normally around species means (Chave et al., 2009, Kattge et al., 2011), both uncertainties could be propagated in a relatively simple way.

The main limitation of the Canopy Constructor compared to more conventional, regression-based approaches are its computational requirements. On one core of an Intel Skylake 6104 processor at 2.3 GHz, computational burden of the Canopy Constructor was ca. 3 minutes for a simulation of the typical field inventory in this study (~10ha), with moderate memory needs (~300 MB). For the full set of 10,000 simulations tested here, this amounted to ~400 cpu core hours per plot for allometric inference and ~700 cpu core hours for reconstructing tree-by-tree assemblies at the landscape scale. Reduced sets of simulations yielded nearly identical results, with very low standard deviations of the estimates (typically 1-2%, and always lower than 5%) but on our hardware, the approach still required 50-100 cpu core hours for a typical data configuration. The procedure is thus beyond desktop computers at the moment, but since simulations within step 1 or step 2 are fully independent, the inference procedure can be parallelized and is relatively easily executed on a modern cluster.

For future reconstructions, there are a number of ways to reduce the Canopy Constructor's runtime. The computationally most expensive part of the procedure is the creation of precise spatial fits, because it involves the constant swapping of tree crown variation across the whole plot. While this is crucial for spatial predictions of biomass and forest structure, unbiased estimates of allometric scaling relationships may already be possible with the initial, non-optimized canopy reconstruction. In this case, runtime

reduces to a few seconds and becomes executable on a desktop computer or within an R package. Furthermore, the two goodness-of-fit metrics currently employed may not yield the best convergence time towards a spatially accurate canopy reconstruction, and the use of a single, feature-based pattern recognition metric such as Earth Mover's Distance (Rubner et al., 2000) may be preferable. Similarly, the rudimentary rejection-based Approximate Bayesian Computation could also be replaced by sequential approaches that converge more rapidly and can be analyzed with state-of-the-art tools (Csilléry et al., 2012; Nunes and Prangle, 2015).

However, what the Canopy Constructor lacks in computational rapidity, it makes up for in comprehensiveness. Where regression-based predictions address one question at a time, the Canopy Constructor's individual-based approach infers a wide range of canopy features simultaneously, most of which we have not explored in this study (e.g., vertical stratification, tree overtopping, and exposure to wind, variation in tree densities and clustering). Furthermore, the simulation-based approach and its Bayesian framework render the integration of further data sources, such as hyperspectral imaging or photogrammetry, relatively straightforward. Such data could extend the approach even further in space and time and increase its precision (Dalponte and Coomes, 2016; Goodbody et al., 2019; Vaglio Laurin et al., 2014), or make use of species-specific properties to predict variation in leaf functional traits and community composition. The consideration of repeated ALS acquisitions could yield individual-based estimates of mortality and growth. And, since it models every individual tree down to 1 cm dbh, the Canopy Constructor could also be used to calibrate and initialize vegetation models, particularly the individual-based forest TROLL model on which much of its code is based (Maréchaux and Chave, 2017), thus contributing to a model-data synthesis at global scales (Shugart et al., 2015). This could provide a link between existing 3D

reconstruction approaches at local scales (Calders et al., 2018) and their extrapolation in space via ALS.

Conclusion

Tropical forests account for over half of the carbon stored in live tissue (Pan et al., 2011), and mapping these stocks at high resolution is essential to assess the impact of ongoing forest deforestation and degradation (Asner et al., 2010). One major challenge of carbon mapping in tropical regions is that national forest inventories are missing and that natural tropical forests are difficult to monitor using traditional forestry techniques (Schimel et al., 2015). Mapping carbon stocks accurately is of prime importance in global carbon cycle research because tropical deforestation is an important cause of anthropogenic carbon dioxide emissions, and a likely cause of major climatic shifts (Boisier et al., 2015; Nobre et al., 2016). The uncertainty of future anthropogenic pressures and climatic changes in African rain forests (Malhi et al., 2013) as well as the recent acceleration of deforestation in the Amazon can only increase the urgency of providing accurate and repeated methods for carbon stock monitoring (Amigo, 2020).

The Canopy Constructor transforms information available at biomass validation sites (sensu Duncanson et al., 2019) into virtual tree inventories that best match empirically measured forest structure. This creates a unifying framework that brings together traditionally separate fields, such as the demographics of plant communities, their underlying physiological constraints and ecosystem functioning, and its results can be used as input for the upscaling to global scales (Dubayah et al., 2020), for dynamic vegetation modelling (F. J. Fischer et al., 2019) or for radiative transfer studies to test how remote sensing signals interact with vegetation, especially radar applications (Tebaldini et al., 2019). Such methods, creating virtual systems that mirror the

complexity of real systems, considerably increase our ability to predict future vegetation dynamics under increased human pressure and climatic changes.

Declaration of competing interest

The authors declare that they have no known competing financial interests or personal relationships that could have appeared to influence the work reported in this paper.

Acknowledgements

We thank Isabelle Maréchaux for her helpful comments on an initial draft of the manuscript. This work has benefitted from "Investissement d'Avenir" grants managed by Agence Nationale de la Recherche (CEBA, ref. ANR-10-LABX-25-01; ANAEE-France: ANR-11-INBS-0001, TULIP: ANR-10-LABX-0041), from CNES, and from ESA (CCI-Biomass). This work was granted access to the HPC resources of CALMIP supercomputing centre in Toulouse under allocation p17012. In Gabon, CENAREST granted permission and provided personnel to establish and study the Rabi plot. Shell Gabon, the society Compagnie des Bois du Gabon provided financial and logistical support. ForestGEO provided technical advice and funding for fieldwork and data analysis. This is contribution #193 of the Gabon Biodiversity Program.

943 **Literature**

944 Åkerblom, M., Raumonen, P., Mäkipää, R., Kaasalainen, M., 2017. Automatic tree species
945 recognition with quantitative structure models. Remote Sens. Environ. 191, 1–12.
946 https://doi.org/10.1016/j.rse.2016.12.002
947 Amigo, I., 2020. When will the Amazon hit a tipping point? Nature.
948 https://doi.org/10.1038/d41586-020-00508-4
949 Anderson-Teixeira, K.J., Davies, S.J., Bennett, A.C., Gonzalez-Akre, E.B., Muller-Landau,
950 H.C., Joseph Wright, S., Abu Salim, K., Almeyda Zambrano, A.M., Alonso, A., Baltzer,
951 J.L., Basset, Y., Bourg, N.A., Broadbent, E.N., Brockelman, W.Y., Bunyavejchewin, S.,
952 Burslem, D.F.R.P., Butt, N., Cao, M., Cardenas, D., Chuyong, G.B., Clay, K., Cordell, S.,
953 Dattaraja, H.S., Deng, X., Detto, M., Du, X., Duque, A., Erikson, D.L., Ewango, C.E.N.,
954 Fischer, G.A., Fletcher, C., Foster, R.B., Giardina, C.P., Gilbert, G.S., Gunatilleke, N.,
955 Gunatilleke, S., Hao, Z., Hargrove, W.W., Hart, T.B., Hau, B.C.H., He, F., Hoffman, F.M.,
956 Howe, R.W., Hubbell, S.P., Inman-Narahari, F.M., Jansen, P.A., Jiang, M., Johnson, D.J.,
957 Kanzaki, M., Kassim, A.R., Kenfack, D., Kibet, S., Kinnaird, M.F., Korte, L., Kral, K.,
958 Kumar, J., Larson, A.J., Li, Y., Li, X., Liu, S., Lum, S.K.Y., Lutz, J.A., Ma, K., Maddalena,
959 D.M., Makana, J.R., Malhi, Y., Marthews, T., Mat Serudin, R., Mcmahon, S.M., McShea,
960 W.J., Memiaghe, H.R., Mi, X., Mizuno, T., Morecroft, M., Myers, J.A., Novotny, V., de
961 Oliveira, A.A., Ong, P.S., Orwig, D.A., Ostertag, R., den Ouden, J., Parker, G.G., Phillips,
962 R.P., Sack, L., Sainge, M.N., Sang, W., Sri-ngernyuang, K., Sukumar, R., Sun, I.F.,
963 Sungpalee, W., Suresh, H.S., Tan, S., Thomas, S.C., Thomas, D.W., Thompson, J.,
964 Turner, B.L., Uriarte, M., Valencia, R., Vallejo, M.I., Vicentini, A., Vrška, T., Wang,
965 Xihua, Wang, Xugao, Weiblen, G., Wolf, A., Xu, H., Yap, S., Zimmerman, J., 2015a.
966 CTFS-ForestGEO: A worldwide network monitoring forests in an era of global
967 change. Glob. Chang. Biol. 21, 528–549. https://doi.org/10.1111/gcb.12712

968 Anderson-Teixeira, K.J., Mcgarvey, J.C., Muller-Landau, H.C., Park, J.Y., Gonzalez-Akre,
969 E.B., Herrmann, V., Bennett, A.C., So, C. V., Bourg, N.A., Thompson, J.R., Mcmahon,
970 S.M., Mcshea, W.J., 2015b. Size-related scaling of tree form and function in a mixed-
971 age forest. Funct. Ecol. 29, 1587–1602. https://doi.org/10.1111/1365-2435.12470
972 Antin, C., Pélissier, R., Vincent, G., Couteron, P., 2013. Crown allometries are less
973 responsive than stem allometry to tree size and habitat variations in an Indian
974 monsoon forest. Trees - Struct. Funct. 27, 1485–1495.
975 https://doi.org/10.1007/s00468-013-0896-7
976 Asner, G.P., Mascaro, J., 2014. Mapping tropical forest carbon: Calibrating plot estimates
977 to a simple LiDAR metric. Remote Sens. Environ. 140, 614–624.
978 https://doi.org/10.1016/j.rse.2013.09.023
979 Asner, G.P., Powell, G.V.N., Mascaro, J., Knapp, D.E., Clark, J.K., Jacobson, J., Kennedy-
980 Bowdoin, T., Balaji, A., Paez-Acosta, G., Victoria, E., Secada, L., Valqui, M., Hughes,
981 R.F., 2010. High-resolution forest carbon stocks and emissions in the Amazon. Proc.
982 Natl. Acad. Sci. U. S. A. 107, 16738–16742.
983 https://doi.org/10.1073/pnas.1004875107
984 Atkins, J.W., Bohrer, G., Fahey, R.T., Hardiman, B.S., Morin, T.H., Stovall, A.E.L.,
985 Zimmerman, N., Gough, C.M., 2018. Quantifying vegetation and canopy structural
986 complexity from terrestrial LiDAR data using the forestr r package. Methods Ecol.
987 Evol. 9, 2057–2066. https://doi.org/10.1111/2041-210X.13061
988 Aubry-Kientz, M., Dutrieux, R., Ferraz, A., Saatchi, S., Hamraz, H., Williams, J., Coomes, D.,
989 Piboule, A., Vincent, G., 2019. A comparative assessment of the performance of
990 individual tree crowns delineation algorithms from ALS data in tropical forests.
991 Remote Sens. 11. https://doi.org/10.3390/rs11091086
992 Babcock, C., Finley, A.O., Bradford, J.B., Kolka, R., Birdsey, R., Ryan, M.G., 2015. LiDAR

based prediction of forest biomass using hierarchical models with spatially varying coefficients. Remote Sens. Environ. 169, 113–127. https://doi.org/10.1016/j.rse.2015.07.028

Bastin, J.F., Barbier, N., Réjou-Méchain, M., Fayolle, A., Gourlet-Fleury, S., Maniatis, D., De Haulleville, T., Baya, F., Beeckman, H., Beina, D., Couteron, P., Chuyong, G., Dauby, G., Doucet, J.L., Droissart, V., Dufrêne, M., Ewango, C., Gillet, J.F., Gonmadje, C.H., Hart, T., Kavali, T., Kenfack, D., Libalah, M., Malhi, Y., Makana, J.R., Pélissier, R., Ploton, P., Serckx, A., Sonké, B., Stevart, T., Thomas, D.W., De Cannière, C., Bogaert, J., 2015. Seeing Central African forests through their largest trees. Sci. Rep. 5. https://doi.org/10.1038/srep13156

Beirne, C., Miao, Z., Nuñez, C.L., Medjibe, V.P., Saatchi, S., White, L.J.T., Poulsen, J.R., 2019. Landscape-level validation of allometric relationships for carbon stock estimation reveals bias driven by soil type. Ecol. Appl. https://doi.org/10.1002/eap.1987

Blanchard, E., Birnbaum, P., Ibanez, T., Boutreux, T., Antin, C., Ploton, P., Vincent, G., Pouteau, R., Vandrot, H., Hequet, V., Barbier, N., Droissart, V., Sonké, B., Texier, N., Kamdem, N.G., Zebaze, D., Libalah, M., Couteron, P., 2016. Contrasted allometries between stem diameter, crown area, and tree height in five tropical biogeographic areas. Trees - Struct. Funct. 30, 1953–1968. https://doi.org/10.1007/s00468-016-1424-3

Boisier, J.P., Ciais, P., Ducharne, A., Guimberteau, M., 2015. Projected strengthening of Amazonian dry season by constrained climate model simulations. Nat. Clim. Chang. 5, 656–660. https://doi.org/10.1038/nclimate2658

Bohn, F.J., Huth, A., 2017. The importance of forest structure to biodiversity-productivity relationships. R. Soc. Open Sci. 4, 160521. https://doi.org/10.1098/rsos.160521

Calders, K., Newnham, G., Burt, A., Murphy, S., Raumonen, P., Herold, M., Culvenor, D.,

1018 Avitabile, V., Disney, M., Armston, J., Kaasalainen, M., 2015. Nondestructive
1019 estimates of above-ground biomass using terrestrial laser scanning. Methods Ecol.
1020 Evol. 6, 198–208. https://doi.org/10.1111/2041-210X.12301
1021 Calders, K., Origo, N., Burt, A., Disney, M., Nightingale, J., Raumonen, P., Åkerblom, M.,
1022 Malhi, Y., Lewis, P., 2018. Realistic forest stand reconstruction from terrestrial
1023 LiDAR for radiative transfer modelling. Remote Sens. 10, 933.
1024 https://doi.org/10.3390/rs10060933
1025 Cano, I.M., Muller-Landau, H.C., Joseph Wright, S., Bohlman, S.A., Pacala, S.W., 2019.
1026 Tropical tree height and crown allometries for the Barro Colorado Nature
1027 Monument, Panama: A comparison of alternative hierarchical models incorporating
1028 interspecific variation in relation to life history traits. Biogeosciences 16, 847–862.
1029 https://doi.org/10.5194/bg-16-847-2019
1030 Chalom, A., Mandai, C., Prado, P., 2013. Sensitivity analyses: a brief tutorial with
1031 Rpackage pse. Cran.Rstudio.Com 1–14.
1032 Chave, J., Coomes, D., Jansen, S., Lewis, S.L., Swenson, N.G., Zanne, A.E., 2009. Towards a
1033 worldwide wood economics spectrum. Ecol. Lett. 12, 351–366.
1034 https://doi.org/10.1111/j.1461-0248.2009.01285.x
1035 Chave, J., Olivier, J., Bongers, F., Châtelet, P., Forget, P.-M., van der Meer, P., Norden, N.,
1036 Riéra, B., Charles-Dominique, P., 2008a. Above-ground biomass and productivity in
1037 a rain forest of eastern South America. J. Trop. Ecol. 24, 355–366.
1038 https://doi.org/10.1017/s0266467408005075
1039 Chave, J., Réjou-Méchain, M., Búrquez, A., Chidumayo, E., Colgan, M.S., Delitti, W.B.C.,
1040 Duque, A., Eid, T., Fearnside, P.M., Goodman, R.C., Henry, M., Martínez-Yrízar, A.,
1041 Mugasha, W.A., Muller-Landau, H.C., Mencuccini, M., Nelson, B.W., Ngomanda, A.,
1042 Nogueira, E.M., Ortiz-Malavassi, E., Pélissier, R., Ploton, P., Ryan, C.M., Saldarriaga,

J.G., Vieilledent, G., 2014. Improved allometric models to estimate the aboveground biomass of tropical trees. Glob. Chang. Biol. 20, 3177–3190. https://doi.org/10.1111/gcb.12629

Chazdon, R.L., Broadbent, E.N., Rozendaal, D.M.A., Bongers, F., Zambrano, A.M.A., Aide, T.M., Balvanera, P., Becknell, J.M., Boukili, V., Brancalion, P.H.S., Craven, D., Almeida-Cortez, J.S., Cabral, G.A.L., De Jong, B., Denslow, J.S., Dent, D.H., DeWalt, S.J., Dupuy, J.M., Durán, S.M., Espírito-Santo, M.M., Fandino, M.C., César, R.G., Hall, J.S., Hernández-Stefanoni, J.L., Jakovac, C.C., Junqueira, A.B., Kennard, D., Letcher, S.G., Lohbeck, M., Martínez-Ramos, M., Massoca, P., Meave, J.A., Mesquita, R., Mora, F., Muñoz, R., Muscarella, R., Nunes, Y.R.F., Ochoa-Gaona, S., Orihuela-Belmonte, E., Peña-Claros, M., Pérez-García, E.A., Piotto, D., Powers, J.S., Rodríguez-Velazquez, J., Romero-Pérez, I.E., Ruíz, J., Saldarriaga, J.G., Sanchez-Azofeifa, A., Schwartz, N.B., Steininger, M.K., Swenson, N.G., Uriarte, M., Van Breugel, M., Van Der Wal, H., Veloso, M.D.M., Vester, H., Vieira, I.C.G., Bentos, T.V., Williamson, G.B., Poorter, L., 2016. Carbon sequestration potential of second-growth forest regeneration in the Latin American tropics. Sci. Adv. 2, e1501639. https://doi.org/10.1126/sciadv.1501639

Condit, R., 1998. Tropical Forest Census Plots, Tropical Forest Census Plots. https://doi.org/10.1007/978-3-662-03664-8

Coomes, D.A., Asner, G.P., Lewis, S.L., Dalponte, M., Phillips, O.L., Qie, L., Nilus, R., Phua, M.-H., Banin, L.F., Burslem, D.F.R.P., Jucker, T., 2017. Area-based vs tree-centric approaches to mapping forest carbon in Southeast Asian forests from airborne laser scanning data. Remote Sens. Environ. 194, 77–88. https://doi.org/10.1016/j.rse.2017.03.017

Coomes, D.A., Duncan, R.P., Allen, R.B., Truscott, J., 2003. Disturbances prevent stem size-density distributions in natural forests from following scaling relationships. Ecol.

Lett. 6, 980–989. https://doi.org/10.1046/j.1461-0248.2003.00520.x

Csilléry, K., Blum, M.G.B., Gaggiotti, O.E., François, O., 2010. Approximate Bayesian Computation (ABC) in practice. Trends Ecol. Evol. https://doi.org/10.1016/j.tree.2010.04.001

Csilléry, K., François, O., Blum, M.G.B., 2012. Abc: An R package for approximate Bayesian computation (ABC). Methods Ecol. Evol. 3, 475–479. https://doi.org/10.1111/j.2041-210X.2011.00179.x

Dalponte, M., Coomes, D.A., 2016. Tree-centric mapping of forest carbon density from airborne laser scanning and hyperspectral data. Methods Ecol. Evol. 7, 1236–1245. https://doi.org/10.1111/2041-210X.12575

Davis, K.T., Dobrowski, S.Z., Holden, Z.A., Higuera, P.E., Abatzoglou, J.T., 2019. Microclimatic buffering in forests of the future: the role of local water balance. Ecography (Cop.). 42, 1–11. https://doi.org/10.1111/ecog.03836

DeRose, R.J., Long, J.N., 2014. Resistance and Resilience: A Conceptual Framework for Silviculture. For. Sci. 60, 1205–1212. https://doi.org/10.5849/forsci.13-507

Disney, M., 2019. Terrestrial LiDAR: a three-dimensional revolution in how we look at trees. New Phytol. 222, 1736–1741. https://doi.org/10.1111/nph.15517

Dassot, M., Constant, T., Fournier, M., 2011. The use of terrestrial LiDAR technology in forest science: Application fields, benefits and challenges. Ann. For. Sci. 68, 959–974. https://doi.org/10.1007/s13595-011-0102-2

Dowle, M., Srinivasan, A., 2018. data.table: Extension of "data.frame". R package version 1.11.2. https://cran.r-project.org/package=data.table.

Dubayah, R., Blair, J.B., Goetz, S., Fatoyinbo, L., Hansen, M., Healey, S., Hofton, M., Hurtt, G., Kellner, J., Luthcke, S., Armston, J., Tang, H., Duncanson, L., Hancock, S., Jantz, P., Marselis, S., Patterson, P., Qi, W., Silva, C., 2020. The Global Ecosystem Dynamics

Investigation: High-resolution laser ranging of the Earth's forests and topography. Sci. Remote Sens. 100002. https://doi.org/10.1016/j.srs.2020.100002

Duncanson, L., Armston, J., Disney, M., Avitabile, V., Barbier, N., Calders, K., Carter, S., Chave, J., Herold, M., Crowther, T.W., Falkowski, M., Kellner, J.R., Labrière, N., Lucas, R., MacBean, N., McRoberts, R.E., Meyer, V., Næsset, E., Nickeson, J.E., Paul, K.I., Phillips, O.L., Réjou-Méchain, M., Román, M., Roxburgh, S., Saatchi, S., Schepaschenko, D., Scipal, K., Siqueira, P.R., Whitehurst, A., Williams, M., 2019. The Importance of Consistent Global Forest Aboveground Biomass Product Validation. Surv. Geophys. 40, 979–999. https://doi.org/10.1007/s10712-019-09538-8

Engone Obiang, N.L., Kenfack, D., Picard, N., Lutz, J.A., Bissiengou, P., Memiaghe, H.R., Alonso, A., 2019. Determinants of spatial patterns of canopy tree species in a tropical evergreen forest in Gabon. J. Veg. Sci. 30, 929–939. https://doi.org/10.1111/jvs.12778

Farrior, C.E., Bohlman, S.A., Hubbell, S., Pacala, S.W., 2016. Dominance of the suppressed: Power-law size structure in tropical forests. Science 351, 155–157. https://doi.org/10.1126/science.aad0592

Fassnacht, F.E., Latifi, H., Hartig, F., 2018. Using synthetic data to evaluate the benefits of large field plots for forest biomass estimation with LiDAR. Remote Sens. Environ. 213, 115–128. https://doi.org/10.1016/j.rse.2018.05.007

Fatoyinbo, L., Pinto, N., Hofton, M., Simard, M., Blair, B., Saatchi, S., Lou, Y., Dubayah, R., Hensley, S., Armston, J., Duncanson, L., Lavalle, M., 2017. The 2016 NASA AfriSAR campaign: Airborne SAR and Lidar measurements of tropical forest structure and biomass in support of future satellite missions, in: International Geoscience and Remote Sensing Symposium (IGARSS). pp. 4286–4287. https://doi.org/10.1109/IGARSS.2017.8127949

1118 Feldpausch, T.R., Lloyd, J., Lewis, S.L., Brienen, R.J.W., Gloor, M., Monteagudo Mendoza, A.,
1119 Lopez-Gonzalez, G., Banin, L., Abu Salim, K., Affum-Baffoe, K., Alexiades, M., Almeida,
1120 S., Amaral, I., Andrade, A., Aragão, L.E.O.C., Araujo Murakami, A., Arets, E.J.M.,
1121 Arroyo, L., Aymard C., G.A., Baker, T.R., Bánki, O.S., Berry, N.J., Cardozo, N., Chave, J.,
1122 Comiskey, J.A., Alvarez, E., De Oliveira, A., Di Fiore, A., Djagbletey, G., Domingues,
1123 T.F., Erwin, T.L., Fearnside, P.M., França, M.B., Freitas, M.A., Higuchi, N., Honorio C.,
1124 E., Iida, Y., Jiménez, E., Kassim, A.R., Killeen, T.J., Laurance, W.F., Lovett, J.C., Malhi, Y.,
1125 Marimon, B.S., Marimon-Junior, B.H., Lenza, E., Marshall, A.R., Mendoza, C., Metcalfe,
1126 D.J., Mitchard, E.T.A., Neill, D.A., Nelson, B.W., Nilus, R., Nogueira, E.M., Parada, A., S.-
1127 H. Peh, K., Pena Cruz, A., Peñuela, M.C., Pitman, N.C.A., Prieto, A., Quesada, C.A.,
1128 Ramírez, F., Ramírez-Angulo, H., Reitsma, J.M., Rudas, A., Saiz, G., Salomão, R.P.,
1129 Schwarz, M., Silva, N., Silva-Espejo, J.E., Silveira, M., Sonké, B., Stropp, J., Taedoumg,
1130 H.E., Tan, S., Ter Steege, H., Terborgh, J., Torello-Raventos, M., Van Der Heijden,
1131 G.M.F., Vásquez, R., Vilanova, E., Vos, V.A., White, L., Willcock, S., Woell, H., Phillips,
1132 O.L., 2012. Tree height integrated into pantropical forest biomass estimates.
1133 Biogeosciences 9, 3381–3403. https://doi.org/10.5194/bg-9-3381-2012
1134 Ferraz, A., Saatchi, S., Mallet, C., Meyer, V., 2016. Lidar detection of individual tree size in
1135 tropical forests. Remote Sens. Environ. 183, 318–333.
1136 https://doi.org/10.1016/j.rse.2016.05.028
1137 Fischer, F.J., Maréchaux, I., Chave, J., 2019. Improving plant allometry by fusing forest
1138 models and remote sensing. New Phytol. 223, 1159–1165.
1139 https://doi.org/10.1111/nph.15810
1140 Fischer, R., Knapp, N., Bohn, F., Shugart, H.H., Huth, A., 2019. The Relevance of Forest
1141 Structure for Biomass and Productivity in Temperate Forests: New Perspectives for
1142 Remote Sensing. Surv. Geophys. 1–26. https://doi.org/10.1007/s10712-019-

09519-x

Garnier, S., 2018. viridis: Default Color Maps from “matplotlib.” R Packag. version 0.5.1.

Goetz, S.J., Steinberg, D., Betts, M.G., Holmes, R.T., Doran, P.J., Dubayah, R., Hofton, M., 2010. Lidar remote sensing variables predict breeding habitat of a Neotropical migrant bird. Ecology 91, 1569–1576. https://doi.org/10.1890/09-1670.1

Goodbody, T.R.H., Coops, N.C., White, J.C., 2019. Digital Aerial Photogrammetry for Updating Area-Based Forest Inventories: A Review of Opportunities, Challenges, and Future Directions. Curr. For. Reports. https://doi.org/10.1007/s40725-019-00087-2

Grassi, G., House, J., Dentener, F., Federici, S., Den Elzen, M., Penman, J., 2017. The key role of forests in meeting climate targets requires science for credible mitigation. Nat. Clim. Chang. 7, 220–226. https://doi.org/10.1038/nclimate3227

Hartig, F., Calabrese, J.M., Reineking, B., Wiegand, T., Huth, A., 2011. Statistical inference for stochastic simulation models - theory and application. Ecol. Lett. 14, 816–827. https://doi.org/10.1111/j.1461-0248.2011.01640.x

Hartig, F., Dislich, C., Wiegand, T., Huth, A., 2014. Technical note: Approximate bayesian parameterization of a process-based tropical forest model. Biogeosciences 11, 1261–1272. https://doi.org/10.5194/bg-11-1261-2014

Henry, H.A.L., Aarssen, L.W., 1999. The interpretation of stem diameter-height allometry in trees: Biomechanical constraints, neighbour effects, or biased regressions? Ecol. Lett. 2, 89–97. https://doi.org/10.1046/j.1461-0248.1999.22054.x

Hijmans, R.J., 2016. raster: Geographic Data Analysis and Modeling. R package version 2.5-8. R Packag.

Hill, R.W., Holland, P.W., 1977. Two Robust Alternatives to Least-Squares Regression. J. Am. Stat. Assoc. 72, 828–833. https://doi.org/10.2307/2286469

1168 Hurtt, G.C., Dubayah, R., Drake, J., Moorcroft, P.R., Pacala, S.W., Blair, J.B., Fearon, M.G.,
1169 2004. Beyond potential vegetation: Combining lidar data and a height-structured
1170 model for carbon studies. Ecol. Appl. 14, 873–883. https://doi.org/10.1890/02-
1171 5317
1172 Hyyppä, J., Inkinen, M., 1999. Detecting and estimating attributes for single trees using
1173 laser scanner. Photogramm. J. Finl. 16, 27–42.
1174 Inman, H.F., Bradley, E.L., 1989. The Overlapping Coefficient as a Measure of Agreement
1175 Between Probability Distributions and Point Estimation of the Overlap of two
1176 Normal Densities. Commun. Stat. - Theory Methods 18, 3851–3874.
1177 https://doi.org/10.1080/03610928908830127
1178 Isenburg, M., 2018. LAStools - efficient LiDAR processing software.
1179 Jucker, T., Bouriaud, O., Coomes, D.A., 2015. Crown plasticity enables trees to optimize
1180 canopy packing in mixed-species forests. Funct. Ecol. 29, 1078–1086.
1181 https://doi.org/10.1111/1365-2435.12428
1182 Jucker, T., Caspersen, J., Chave, J., Antin, C., Barbier, N., Bongers, F., Dalponte, M., van
1183 Ewijk, K.Y., Forrester, D.I., Haeni, M., Higgins, S.I., Holdaway, R.J., Iida, Y., Lorimer, C.,
1184 Marshall, P.L., Momo, S., Moncrieff, G.R., Ploton, P., Poorter, L., Rahman, K.A.,
1185 Schlund, M., Sonké, B., Sterck, F.J., Trugman, A.T., Usoltsev, V.A., Vanderwel, M.C.,
1186 Waldner, P., Wedeux, B.M.M., Wirth, C., Wöll, H., Woods, M., Xiang, W., Zimmermann,
1187 N.E., Coomes, D.A., 2017. Allometric equations for integrating remote sensing
1188 imagery into forest monitoring programmes. Glob. Chang. Biol. 23, 177–190.
1189 https://doi.org/10.1111/gcb.13388
1190 Kattge, J., Díaz, S., Lavorel, S., Prentice, I.C., Leadley, P., Bönisch, G., Garnier, E., Westoby,
1191 M., Reich, P.B., Wright, I.J., Cornelissen, J.H.C., Violle, C., Harrison, S.P., Van Bodegom,
1192 P.M., Reichstein, M., Enquist, B.J., Soudzilovskaia, N.A., Ackerly, D.D., Anand, M.,

Atkin, O., Bahn, M., Baker, T.R., Baldocchi, D., Bekker, R., Blanco, C.C., Blonder, B., Bond, W.J., Bradstock, R., Bunker, D.E., Casanoves, F., Cavender-Bares, J., Chambers, J.Q., Chapin, F.S., Chave, J., Coomes, D., Cornwell, W.K., Craine, J.M., Dobrin, B.H., Duarte, L., Durka, W., Elser, J., Esser, G., Estiarte, M., Fagan, W.F., Fang, J., Fernández-Méndez, F., Fidelis, A., Finegan, B., Flores, O., Ford, H., Frank, D., Freschet, G.T., Fyllas, N.M., Gallagher, R. V., Green, W.A., Gutierrez, A.G., Hickler, T., Higgins, S.I., Hodgson, J.G., Jalili, A., Jansen, S., Joly, C.A., Kerkhoff, A.J., Kirkup, D., Kitajima, K., Kleyer, M., Klotz, S., Knops, J.M.H., Kramer, K., Kühn, I., Kurokawa, H., Laughlin, D., Lee, T.D., Leishman, M., Lens, F., Lenz, T., Lewis, S.L., Lloyd, J., Llusià, J., Louault, F., Ma, S., Mahecha, M.D., Manning, P., Massad, T., Medlyn, B.E., Messier, J., Moles, A.T., Müller, S.C., Nadrowski, K., Naeem, S., Niinemets, Ü., Nöllert, S., Nüske, A., Ogaya, R., Oleksyn, J., Onipchenko, V.G., Onoda, Y., Ordoñez, J., Overbeck, G., Ozinga, W.A., Patiño, S., Paula, S., Pausas, J.G., Peñuelas, J., Phillips, O.L., Pillar, V., Poorter, H., Poorter, L., Poschlod, P., Prinzing, A., Proulx, R., Rammig, A., Reinsch, S., Reu, B., Sack, L., Salgado-Negret, B., Sardans, J., Shiodera, S., Shipley, B., Siefert, A., Sosinski, E., Soussana, J.F., Swaine, E., Swenson, N., Thompson, K., Thornton, P., Waldram, M., Weiher, E., White, M., White, S., Wright, S.J., Yguel, B., Zaehle, S., Zanne, A.E., Wirth, C., 2011. TRY - a global database of plant traits. Glob. Chang. Biol. 17, 2905–2935. https://doi.org/10.1111/j.1365-2486.2011.02451.x

Khosravipour, A., Skidmore, A.K., Isenburg, M., Wang, T., Hussin, Y.A., 2014. Generating Pit-free Canopy Height Models from Airborne Lidar. Photogramm. Eng. Remote Sens. 80, 863–872. https://doi.org/10.14358/PERS.80.9.863

King, D.A., 1996. Allometry and life history of tropical trees. J. Trop. Ecol. 12, 25–44. https://doi.org/10.1017/s0266467400009299

Knapp, N., Fischer, R., Huth, A., 2018. Linking lidar and forest modeling to assess

biomass estimation across scales and disturbance states. Remote Sens. Environ. 205, 199–209. https://doi.org/10.1016/j.rse.2017.11.018

Labriere, N., Tao, S., Chave, J., Scipal, K., Toan, T. Le, Abernethy, K., Alonso, A., Barbier, N., Bissiengou, P., Casal, T., Davies, S.J., Ferraz, A., Herault, B., Jaouen, G., Jeffery, K.J., Kenfack, D., Korte, L., Lewis, S.L., Malhi, Y., Memiaghe, H.R., Poulsen, J.R., Rejou-Mechain, M., Villard, L., Vincent, G., White, L.J.T., Saatchi, S., 2018. In Situ Reference Datasets from the TropiSAR and AfriSAR Campaigns in Support of Upcoming Spaceborne Biomass Missions. IEEE J. Sel. Top. Appl. Earth Obs. Remote Sens. 11, 3617–3627. https://doi.org/10.1109/JSTARS.2018.2851606

Lau, A., Martius, C., Bartholomeus, H., Shenkin, A., Jackson, T., Malhi, Y., Herold, M., Bentley, L.P., 2019. Estimating architecture-based metabolic scaling exponents of tropical trees using terrestrial LiDAR and 3D modelling. For. Ecol. Manage. 439, 132–145. https://doi.org/10.1016/j.foreco.2019.02.019

Laurance, W.F., Nascimento, H.E.M., Laurance, S.G., Andrade, A., Ribeiro, J.E.L.S., Giraldo, J.P., Lovejoy, T.E., Condit, R., Chave, J., Harms, K.E., D'Angelo, S., 2006. Rapid decay of tree-community composition in Amazonian forest fragments. Proc. Natl. Acad. Sci. U. S. A. 103, 19010–19014. https://doi.org/10.1073/pnas.0609048103

Le Toan, T., Quegan, S., Davidson, M.W.J., Balzter, H., Paillou, P., Papathanassiou, K., Plummer, S., Rocca, F., Saatchi, S., Shugart, H., Ulander, L., 2011. The BIOMASS mission: Mapping global forest biomass to better understand the terrestrial carbon cycle. Remote Sens. Environ. 115, 2850–2860. https://doi.org/10.1016/j.rse.2011.03.020

Levick, S.R., Asner, G.P., 2013. The rate and spatial pattern of treefall in a savanna landscape. Biol. Conserv. 157, 121–127. https://doi.org/10.1016/j.biocon.2012.07.009

1243 Lewis, S.L., Edwards, D.P., Galbraith, D., 2015. Increasing human dominance of tropical
1244 forests. Science 349, 827 – 832. https://doi.org/10.1126/science.aaa9932
1245 Lines, E.R., Zavala, M.A., Purves, D.W., Coomes, D.A., 2012. Predictable changes in
1246 aboveground allometry of trees along gradients of temperature, aridity and
1247 competition. Glob. Ecol. Biogeogr. 21, 1017–1028. https://doi.org/10.1111/j.1466-
1248 8238.2011.00746.x
1249 Lutz, J.A., Furniss, T.J., Johnson, D.J., Davies, S.J., Allen, D., Alonso, A., Anderson-Teixeira,
1250 K.J., Andrade, A., Baltzer, J., Becker, K.M.L., Blomdahl, E.M., Bourg, N.A.,
1251 Bunyavejchewin, S., Burslem, D.F.R.P., Cansler, C.A., Cao, K., Cao, M., Cárdenas, D.,
1252 Chang, L.W., Chao, K.J., Chao, W.C., Chiang, J.M., Chu, C., Chuyong, G.B., Clay, K.,
1253 Condit, R., Cordell, S., Dattaraja, H.S., Duque, A., Ewango, C.E.N., Fischer, G.A.,
1254 Fletcher, C., Freund, J.A., Giardina, C., Germain, S.J., Gilbert, G.S., Hao, Z., Hart, T., Hau,
1255 B.C.H., He, F., Hector, A., Howe, R.W., Hsieh, C.F., Hu, Y.H., Hubbell, S.P., Inman-
1256 Narahari, F.M., Itoh, A., Janík, D., Kassim, A.R., Kenfack, D., Korte, L., Král, K., Larson,
1257 A.J., Li, Y. De, Lin, Y., Liu, S., Lum, S., Ma, K., Makana, J.R., Malhi, Y., McMahon, S.M.,
1258 McShea, W.J., Memiaghe, H.R., Mi, X., Morecroft, M., Musili, P.M., Myers, J.A., Novotny,
1259 V., de Oliveira, A., Ong, P., Orwig, D.A., Ostertag, R., Parker, G.G., Patankar, R., Phillips,
1260 R.P., Reynolds, G., Sack, L., Song, G.Z.M., Su, S.H., Sukumar, R., Sun, I.F., Suresh, H.S.,
1261 Swanson, M.E., Tan, S., Thomas, D.W., Thompson, J., Uriarte, M., Valencia, R.,
1262 Vicentini, A., Vrška, T., Wang, X., Weiblen, G.D., Wolf, A., Wu, S.H., Xu, H., Yamakura,
1263 T., Yap, S., Zimmerman, J.K., 2018. Global importance of large-diameter trees. Glob.
1264 Ecol. Biogeogr. 27, 849–864. https://doi.org/10.1111/geb.12747
1265 Lutz, J.A., Larson, A.J., Freund, J.A., Swanson, M.E., Bible, K.J., 2013. The importance of
1266 large-diameter trees to forest structural heterogeneity. PLoS One 8.
1267 https://doi.org/10.1371/journal.pone.0082784

1268 Maréchaux, I., Chave, J., 2017. An individual-based forest model to jointly simulate
1269 carbon and tree diversity in Amazonia: description and applications. Ecol. Monogr.
1270 87, 632–664. https://doi.org/10.1002/ecm.1271
1271 Mascaro, J., Detto, M., Asner, G.P., Muller-Landau, H.C., 2011. Evaluating uncertainty in
1272 mapping forest carbon with airborne LiDAR. Remote Sens. Environ. 115, 3770–
1273 3774. https://doi.org/10.1016/j.rse.2011.07.019
1274 Malhi, Y., Adu-Bredu, S., Asare, R.A., Lewis, S.L., Mayaux, P., 2013. African rainforests:
1275 Past, present and future. Philos. Trans. R. Soc. B Biol. Sci.
1276 https://doi.org/10.1098/rstb.2012.0312
1277 Memiaghe, H.R., Lutz, J.A., Korte, L., Alonso, A., Kenfack, D., 2016. Ecological Importance
1278 of Small-Diameter Trees to the Structure, Diversity and Biomass of a Tropical
1279 Evergreen Forest at Rabi, Gabon. PLoS One 11.
1280 https://doi.org/10.1371/journal.pone.0154988
1281 Meyer, V., Saatchi, S., Clark, D.B., Keller, M., Vincent, G., Ferraz, A., Espírito-Santo, F.,
1282 D'Oliveira, M.V.N., Kaki, D., Chave, J., 2018. Canopy Area of Large Trees Explains
1283 Aboveground Biomass Variations across Nine Neotropical Forest Landscapes.
1284 Biogeosciences Discuss. 1–38. https://doi.org/10.5194/bg-2017-547
1285 Molto, Q., Hérault, B., Boreux, J.J., Daullet, M., Rousteau, A., Rossi, V., 2014. Predicting tree
1286 heights for biomass estimates in tropical forests -A test from French Guiana.
1287 Biogeosciences 11, 3121–3130. https://doi.org/10.5194/bg-11-3121-2014
1288 Momo Takoudjou, S., Ploton, P., Sonké, B., Hackenberg, J., Griffon, S., Coligny, F., Kamdem,
1289 N.G., Libalah, M., Mofack, G.I.I., Le Moguédec, G., Pélissier, R., Barbier, N., 2017. Using
1290 terrestrial laser scanning data to estimate large tropical trees biomass and calibrate
1291 allometric models: A comparison with traditional destructive approach. Methods
1292 Ecol. Evol. 9, 905–916. https://doi.org/10.1111/2041-210X.12933

1293 Morsdorf, F., Meier, E., Kötz, B., Itten, K.I., Dobbertin, M., Allgöwer, B., 2004. LIDAR-based
1294 geometric reconstruction of boreal type forest stands at single tree level for forest
1295 and wildland fire management, in: Remote Sensing of Environment. pp. 353–362.
1296 https://doi.org/10.1016/j.rse.2004.05.013
1297 Muller-Landau, H.C., Condit, R.S., Harms, K.E., Marks, C.O., Thomas, S.C., Bunyavejchewin,
1298 S., Chuyong, G., Co, L., Davies, S., Foster, R., Gunatilleke, S., Gunatilleke, N., Hart, T.,
1299 Hubbell, S.P., Itoh, A., Kassim, A.R., Kenfack, D., LaFrankie, J. V., Lagunzad, D., Lee,
1300 H.S., Losos, E., Makana, J.R., Ohkubo, T., Samper, C., Sukumar, R., Sun, I.F., Nur
1301 Supardi, M.N., Tan, S., Thomas, D., Thompson, J., Valencia, R., Vallejo, M.I., Muñoz,
1302 G.V., Yamakura, T., Zimmerman, J.K., Dattaraja, H.S., Esufali, S., Hall, P., He, F.,
1303 Hernandez, C., Kiratiprayoon, S., Suresh, H.S., Wills, C., Ashton, P., 2006. Comparing
1304 tropical forest tree size distributions with the predictions of metabolic ecology and
1305 equilibrium models. Ecol. Lett. 9, 589–602. https://doi.org/10.1111/j.1461-
1306 0248.2006.00915.x
1307 Næsset, E., 2002. Predicting forest stand characteristics with airborne scanning laser
1308 using a practical two-stage procedure and field data. Remote Sens. Environ. 80, 88–
1309 99. https://doi.org/10.1016/S0034-4257(01)00290-5
1310 Newnham, G.J., Armston, J.D., Calders, K., Disney, M.I., Lovell, J.L., Schaaf, C.B., Strahler,
1311 A.H., Mark Danson, F., 2015. Terrestrial laser scanning for plot-scale forest
1312 measurement. Curr. For. Reports 1, 239–251. https://doi.org/10.1007/s40725-
1313 015-0025-5
1314 Niklas, K.J., 1994. Plant allometry: the scaling of form and process. University of Chicago
1315 Press.
1316 Niklas, K.J., 2007. Maximum plant height and the biophysical factors that limit it, in: Tree
1317 Physiology. pp. 433–440. https://doi.org/10.1093/treephys/27.3.433

1318 Niklas, K.J., Midgley, J.J., Enquist, B.J., 2003. A general model for mass-growth-density
1319 relations across tree-dominated communities. Evol. Ecol. Res. 5, 459–468.
1320 Nobre, C.A., Sampaio, G., Borma, L.S., Castilla-Rubio, J.C., Silva, J.S., Cardoso, M., 2016.
1321 Land-use and climate change risks in the amazon and the need of a novel
1322 sustainable development paradigm. Proc. Natl. Acad. Sci. U. S. A. 113, 10759–10768.
1323 https://doi.org/10.1073/pnas.1605516113
1324 Nunes, M., Prangle, D., 2015. abctools : An R Package for Tuning Approximate Bayesian
1325 Computation Analyses. R J. 7, 1–16.
1326 Oldeman, R., 1974. The architecture of the forest of French Guiana. L'architecture de la
1327 foret Guyanaise, Memoires-ORSTOM. ORSTOM.
1328 Palace, M.W., Sullivan, F.B., Ducey, M.J., Treuhaft, R.N., Herrick, C., Shimbo, J.Z., Mota-E-
1329 Silva, J., 2015. Estimating forest structure in a tropical forest using field
1330 measurements, a synthetic model and discrete return lidar data. Remote Sens.
1331 Environ. 161, 1–11. https://doi.org/10.1016/j.rse.2015.01.020
1332 Pan, Y., Birdsey, R.A., Fang, J., Houghton, R., Kauppi, P.E., Kurz, W.A., Phillips, O.L.,
1333 Shvidenko, A., Lewis, S.L., Canadell, J.G., Ciais, P., Jackson, R.B., Pacala, S.W., McGuire,
1334 A.D., Piao, S., Rautiainen, A., Sitch, S., Hayes, D., 2011. A Large and Persistent Carbon
1335 Sink in the World's Forests. Science (80-.). 333, 988 LP – 993.
1336 https://doi.org/10.1126/science.1201609
1337 Pan, Y., Birdsey, R.A., Phillips, O.L., Jackson, R.B., 2013. The Structure, Distribution, and
1338 Biomass of the World's Forests. Annu. Rev. Ecol. Evol. Syst. 44, 593–622.
1339 https://doi.org/10.1146/annurev-ecolsys-110512-135914
1340 Poncy, O., Sabatier, D., Prévost, M.F., Hardy, I., 2001. The Lowland High Rainforest:
1341 Structure and Tree Species Diversity, in: Bongers, F., Charles-Dominique, P., Forget,
1342 P.M., Théry, M. (Eds.), Nouragues. Monographiae Biologicae, Vol 80. Springer,

1343 Dordrecht, pp. 31–46.
1344 Poorter, L., Bongers, L., Bongers, F., 2006. Architecture of 54 moist-forest tree species:
1345 Traits, trade-offs, and functional groups. Ecology 87, 1289–1301.
1346 Pretzsch, H., 2014. Canopy space filling and tree crown morphology in mixed-species
1347 stands compared with monocultures. For. Ecol. Manage. 327, 251–264.
1348 https://doi.org/10.1016/j.foreco.2014.04.027
1349 Pretzsch, H., Dieler, J., 2012. Evidence of variant intra- and interspecific scaling of tree
1350 crown structure and relevance for allometric theory. Oecologia 169, 637–649.
1351 https://doi.org/10.1007/s00442-011-2240-5
1352 Purves, D.W., Lichstein, J.W., Strigul, N., Pacala, S.W., 2008. Predicting and understanding
1353 forest dynamics using a simple tractable model. Proc. Natl. Acad. Sci. 105, 17018–
1354 17022. https://doi.org/10.1073/pnas.0807754105
1355 Pyörälä, J., Saarinen, N., Kankare, V., Coops, N.C., Liang, X., Wang, Y., Holopainen, M.,
1356 Hyyppä, J., Vastaranta, M., 2019. Variability of wood properties using airborne and
1357 terrestrial laser scanning. Remote Sens. Environ. 235.
1358 https://doi.org/10.1016/j.rse.2019.111474
1359 R Development Core Team, 2019. R: A Language and Environment for Statistical
1360 Computing. R Found. Stat. Comput. https://doi.org/10.1007/978-3-540-74686-7
1361 Réjou-Méchain, M., Muller-Landau, H.C., Detto, M., Thomas, S.C., Le Toan, T., Saatchi, S.S.,
1362 Barreto-Silva, J.S., Bourg, N.A., Bunyavejchewin, S., Butt, N., Brockelman, W.Y., Cao,
1363 M., Cárdenas, D., Chiang, J.M., Chuyong, G.B., Clay, K., Condit, R., Dattaraja, H.S.,
1364 Davies, S.J., Duque, A., Esufali, S., Ewango, C., Fernando, R.H.S., Fletcher, C.D., N.
1365 Gunatilleke, I.A.U., Hao, Z., Harms, K.E., Hart, T.B., Hérault, B., Howe, R.W., Hubbell,
1366 S.P., Johnson, D.J., Kenfack, D., Larson, A.J., Lin, L., Lin, Y., Lutz, J.A., Makana, J.R.,
1367 Malhi, Y., Marthews, T.R., Mcewan, R.W., Mcmahon, S.M., Mcshea, W.J., Muscarella,

1368 R., Nathalang, A., Noor, N.S.M., Nytch, C.J., Oliveira, A.A., Phillips, R.P.,
1369 Pongpattananurak, N., Punchi-Manage, R., Salim, R., Schurman, J., Sukumar, R.,
1370 Suresh, H.S., Suwanvecho, U., Thomas, D.W., Thompson, J., Uríarte, M., Valencia, R.,
1371 Vicentini, A., Wolf, A.T., Yap, S., Yuan, Z., Zartman, C.E., Zimmerman, J.K., Chave, J.,
1372 2014. Local spatial structure of forest biomass and its consequences for remote
1373 sensing of carbon stocks. Biogeosciences 11, 6827–6840.
1374 https://doi.org/10.5194/bg-11-6827-2014
1375 Réjou-Méchain, M., Tanguy, A., Piponiot, C., Chave, J., Hérault, B., 2017. Biomass: an R
1376 Package for Estimating Above-Ground Biomass and Its Uncertainty in Tropical
1377 Forests. Methods Ecol. Evol. 8, 1163–1167. https://doi.org/10.1111/2041-
1378 210X.12753
1379 Réjou-Méchain, M., Tymen, B., Blanc, L., Fauset, S., Feldpausch, T.R., Monteagudo, A.,
1380 Phillips, O.L., Richard, H., Chave, J., 2015. Using repeated small-footprint LiDAR
1381 acquisitions to infer spatial and temporal variations of a high-biomass Neotropical
1382 forest. Remote Sens. Environ. 169, 93–101.
1383 https://doi.org/10.1016/j.rse.2015.08.001
1384 Riaño, D., Valladares, F., Condés, S., Chuvieco, E., 2004. Estimation of leaf area index and
1385 covered ground from airborne laser scanner (Lidar) in two contrasting forests.
1386 Agric. For. Meteorol. 124, 269–275.
1387 https://doi.org/10.1016/j.agrformet.2004.02.005
1388 Rosette, J.A.B., North, P.R.J., Suárez, J.C., 2008. Vegetation height estimates for a mixed
1389 temperate forest using satellite laser altimetry, in: International Journal of Remote
1390 Sensing. pp. 1475–1493. https://doi.org/10.1080/01431160701736380
1391 Rubner, Y., Tomasi, C., Guibas, L.J., 2000. Earth mover's distance as a metric for image
1392 retrieval. Int. J. Comput. Vis. 40, 99–121.

https://doi.org/10.1023/A:1026543900054

Schimel, D., Pavlick, R., Fisher, J.B., Asner, G.P., Saatchi, S., Townsend, P., Miller, C., Frankenberg, C., Hibbard, K., Cox, P., 2015. Observing terrestrial ecosystems and the carbon cycle from space. Glob. Chang. Biol. https://doi.org/10.1111/gcb.12822

Seidl, R., Rammer, W., Spies, T.A., 2014. Disturbance legacies increase the resilience of forest ecosystem structure, composition, and functioning. Ecol. Appl. 24, 2063–2077. https://doi.org/10.1890/14-0255.1

Shugart, H.H., Asner, G.P., Fischer, R., Huth, A., Knapp, N., Le Toan, T., Shuman, J.K., 2015. Computer and remote-sensing infrastructure to enhance large-scale testing of individual-based forest models. Front. Ecol. Environ. 13, 503–511. https://doi.org/10.1890/140327

Shugart, H.H., Saatchi, S., Hall, F.G., 2010. Importance of structure and its measurement in quantifying function of forest ecosystems. J. Geophys. Res. Biogeosciences 115, G2. https://doi.org/10.1029/2009JG000993

Spriggs, R.A., Vanderwel, M.C., Jones, T.A., Caspersen, J.P., Coomes, D.A., 2019. A critique of general allometry-inspired models for estimating forest carbon density from airborne LiDAR. PLoS One 14, e0215238. https://doi.org/10.1371/journal.pone.0215238

Spriggs, R.A., Vanderwel, M.C., Jones, T.A., Caspersen, J.P., Coomes, D.A., 2015. A simple area-based model for predicting airborne LiDAR first returns from stem diameter distributions: An example study in an uneven-aged, mixed temperate forest. Can. J. For. Res. 45, 1338–1350. https://doi.org/10.1139/cjfr-2015-0018

Sterck, F.J., Bongers, F., 2001. Crown development in tropical rain forest trees: Patterns with tree height and light availability. J. Ecol. 89, 1–13. https://doi.org/10.1046/j.1365-2745.2001.00525.x

1418 Stovall, A.E.L., Anderson-Teixeira, K.J., Shugart, H.H., 2018. Assessing terrestrial laser
1419 scanning for developing non-destructive biomass allometry. For. Ecol. Manage. 427,
1420 217–229. https://doi.org/10.1016/j.foreco.2018.06.004
1421 Stovall, A.E.L., Shugart, H., Yang, X., 2019. Tree height explains mortality risk during an
1422 intense drought. Nat. Commun. 10. https://doi.org/10.1038/s41467-019-12380-6
1423 Strigul, N., Pristinski, D., Purves, D., Dushoff, J., Pacala, S., 2008. Scaling from trees to
1424 forests: Tractable macroscopic equations for forest dynamics. Ecol. Monogr. 78,
1425 523–545. https://doi.org/10.1890/08-0082.1
1426 Sullivan, M.J.P., Lewis, S.L., , W., Qie, L., Baker, T.R., Banin, L.F., Chave, J., Cuni-Sanchez, A.,
1427 Feldpausch, T.R., Lopez-Gonzalez, G., Arets, E., Ashton, P., Bastin, J.F., Berry, N.J.,
1428 Bogaert, J., Boot, R., Brearley, F.Q., Brienen, R., Burslem, D.F.R.P., de Canniere, C.,
1429 Chudomelová, M., Dančák, M., Ewango, C., Hédl, R., Lloyd, J., Makana, J.R., Malhi, Y.,
1430 Marimon, B.S., Junior, B.H.M., Metali, F., Moore, S., Nagy, L., Vargas, P.N., Pendry, C.A.,
1431 Ramírez-Angulo, H., Reitsma, J., Rutishauser, E., Salim, K.A., Sonké, B., Sukri, R.S.,
1432 Sunderland, T., Svátek, M., Umunay, P.M., Martinez, R.V., Vernimmen, R.R.E., Torre,
1433 E.V., Vleminckx, J., Vos, V., Phillips, O.L., 2018. Field methods for sampling tree
1434 height for tropical forest biomass estimation. Methods Ecol. Evol. 9, 1179–1189.
1435 https://doi.org/10.1111/2041-210X.12962
1436 Swain, M.J., Ballard, D.H., 1991. Color indexing. Int. J. Comput. Vis. 7, 11–32.
1437 https://doi.org/10.1007/BF00130487
1438 Tanskanen, H., Venäläinen, A., Puttonen, P., Granström, A., 2005. Impact of stand
1439 structure on surface fire ignition potential in Picea abies and Pinus sylvestris
1440 forests in southern Finland. Can. J. For. Res. 35, 410–420.
1441 https://doi.org/10.1139/x04-188
1442 Taubert, F., Jahn, M.W., Dobner, H.-J., Wiegand, T., Huth, A., 2015. The structure of

1443 tropical forests and sphere packings. Proc. Natl. Acad. Sci. 112, 15125–15129.
1444 https://doi.org/10.1073/pnas.1513417112
1445 Tebaldini, S., Ho Tong Minh, D., Mariotti d'Alessandro, M., Villard, L., Le Toan, T., Chave,
1446 J., 2019. The Status of Technologies to Measure Forest Biomass and Structural
1447 Properties: State of the Art in SAR Tomography of Tropical Forests. Surv. Geophys.
1448 https://doi.org/10.1007/s10712-019-09539-7
1449 Ter Steege, H., Pitman, N.C.A., Phillips, O.L., Chave, J., Sabatier, D., Duque, A., Molino, J.F.,
1450 Prévost, M.F., Spichiger, R., Castellanos, H., Von Hildebrand, P., Vásquez, R., 2006.
1451 Continental-scale patterns of canopy tree composition and function across
1452 Amazonia. Nature 443, 444–447. https://doi.org/10.1038/nature05134
1453 Thomas, S.C., 1996. Asymptotic height as a predictor of growth and allometric
1454 characteristics in Malaysian rain forest trees. Am. J. Bot. 83, 556–566.
1455 https://doi.org/10.2307/2445913
1456 Vaglio Laurin, G., Chen, Q., Lindsell, J.A., Coomes, D.A., Frate, F. Del, Guerriero, L., Pirotti,
1457 F., Valentini, R., 2014. Above ground biomass estimation in an African tropical
1458 forest with lidar and hyperspectral data. ISPRS J. Photogramm. Remote Sens. 89,
1459 49–58. https://doi.org/10.1016/j.isprsjprs.2014.01.001
1460 Van Leeuwen, M., Hilker, T., Coops, N.C., Frazer, G., Wulder, M.A., Newnham, G.J.,
1461 Culvenor, D.S., 2011. Assessment of standing wood and fiber quality using ground
1462 and airborne laser scanning: A review. For. Ecol. Manage.
1463 https://doi.org/10.1016/j.foreco.2011.01.032
1464 Vincent, G., Antin, C., Laurans, M., Heurtebize, J., Durrieu, S., Lavalley, C., Dauzat, J., 2017.
1465 Mapping plant area index of tropical evergreen forest by airborne laser scanning. A
1466 cross-validation study using LAI2200 optical sensor. Remote Sens. Environ. 198,
1467 254–266. https://doi.org/10.1016/j.rse.2017.05.034

West, G.B., Brown, J.H., Enquist, B.J., 1999. A general model for the structure and allometry of plant vascular systems. Nature 400, 664–667. https://doi.org/10.1038/23251

West, G.B., Enquist, B.J., Brown, J.H., 2009. A general quantitative theory of forest structure and dynamics. Proc. Natl. Acad. Sci. U. S. A. 106, 7040–7045. https://doi.org/10.1073/pnas.0812294106

Wickham, H., 2011. ggplot2. Wiley Interdiscip. Rev. Comput. Stat. https://doi.org/10.1002/wics.147

Zanne, A.E., Lopez-Gonzalez, G., Coomes, D.A., Ilic, J., Jansen, S., Lewis, S.L., Miller, R.B., Swenson, N.G., Wiemann, M.C., Chave, J., 2009. Data from: Global wood density database. Dryad Digit. Repos. https://doi.org/10.5061/dryad.234

Zolkos, S.G., Goetz, S.J., Dubayah, R., 2013. A meta-analysis of terrestrial aboveground biomass estimation using lidar remote sensing. Remote Sens. Environ. 128, 289–298. https://doi.org/10.1016/j.rse.2012.10.017

List of Figure Captions

Figure 1: The two-step procedure of the Canopy Constructor algorithm. Step 1 uses tree inventory data, and a canopy height model (CHM). To infer the position and size of each tree, the algorithm creates an initial reconstruction drawing randomly dimensions from allometric relationships between tree dimensions. In ill-fitting regions (red), deviations from the allometric means are swapped between trees until a good spatial fit is obtained (green). Step 2 extrapolates the results of step 1 and creates virtual inventories across thousands of hectares, following the same fitting algorithm as in step 1, but with fitted trees drawn from a distribution (see main text for details).

Figure 2: Example of canopy reconstruction at the Petit Plateau plot, Nouragues. Shown are the initial canopy height model (CHM) where tree dimensions are randomly drawn from site-specific allometries (a), the ALS-derived CHM (b), and the final reconstruction of the Canopy Constructor (c).

Figure 3: Inferred allometries at Nouragues and Rabi (step 1). The panels show height allometries (top row) and crown allometries (bottom row), as inferred by the Canopy Constructor, for Nouragues (a,d), Rabi (b,e) and both sites combined (c,f). The grey background indicates the prior range. Mean and 75% highest density intervals are given for each plot separately, i.e. for Grand Plateau (orange) and Petit Plateau (dark red) at Nouragues, and for the 10ha (light blue) and 15ha (dark blue) plot at Rabi. As comparison, we have plotted empirical height allometries measured from in the field for both Grand Plateau (dotted) and Petit Plateau (dashed) in the top panels, as well as a single ground-inferred allometry at Rabi (dotted). Results for same inference procedure, but with a lower number of simulation runs, are provided in Figure S8.

Figure 4: Aboveground biomass predictions for ALS campaign at Nouragues and Rabi (step 2). Maps show the mean aboveground biomass values (t ha-1) predicted with the Canopy Constructor approach across 2,016 ha at Nouragues (panel a) and 832 ha at Rabi (panel d), as well as the respective coefficient of variation across 100 simulations (panels b and e, dimensionless). Also given are the overall distributions of aboveground biomass (panels c and f, red distributions, in t ha-1) and previously obtained estimates (panels c and f, yellow) from a pooled regression-model (Labrière et al. 2018). Clearly evident is the shrinkage towards the mean in the regression-based approach, as opposed to much stronger variation in the Canopy Constructor approach. Please note that the geographic extent of the maps has been rescaled for visualization purposes.

Figure 5: Evaluation of aboveground biomass predictions in extrapolation (step 2). Shown are the predictions of aboveground biomass (median of 100 posterior simulations, given in t ha^{-1}) at the 1 ha scale (a, b) and 0.25 ha scale (c, d). The left column shows the results when the space-filling approach is applied at the calibration plot from which allometries and packing densities were derived ("Model fit"), the right column the results when the approach is transferred between plots ("Cross-validation"). The Nouragues results are plotted in red/orange, and for Rabi in dark/light green. Goodness of fit values are provided in the bottom-right corner of the panels. MBE does not change between 0.25 and 1 ha scales and is thus only given in the top panels. For visualization purposes, we only plot error bars at the hectare scale, representing the interquartile ranges of estimates from 100 posterior simulations.